Report No. K-TRAN: KU-21-2 ▪ FINAL REPORT ▪ August 2023

Pullout Resistance of Reinforcement of Lightweight Cellular Concrete Fill

Jie Han, Ph.D., P.E., F.ASCE
Yuqiu Ye, M.S.
Robert L. Parsons, Ph.D., P.E.
Matt O'Reilly, Ph.D., P.E.
Hao Liu, Ph.D.

The University of Kansas

Kansas Department of Transportation

1 Report No. K-TRAN: KU-21-2	**2 Government Accession No.**	**3 Recipient Catalog No.**
4 Title and Subtitle Pullout Resistance of Reinforcement of Lightweight Cellular Concrete Fill		**5 Report Date** August 2023 **6 Performing Organization Code**
7 Author(s) Jie Han, Ph.D., P.E., F.ASCE, Yuqiu Ye, M.S., Robert L. Parsons, Ph.D., P.E., Matt O'Reilly, Ph.D., P.E., Hao Liu, Ph.D.		**8 Performing Organization Report No.**
9 Performing Organization Name and Address The University of Kansas Department of Civil, Environmental & Architectural Engineering 1530 West 15th St Lawrence, Kansas 66045-7609		**10 Work Unit No. (TRAIS)** **11 Contract or Grant No.** C2169
12 Sponsoring Agency Name and Address Kansas Department of Transportation Bureau of Research 2300 SW Van Buren Topeka, Kansas 66611-1195		**13 Type of Report and Period Covered** Final Report July 2020 – June 2022 **14 Sponsoring Agency Code** RE-0814-01
15 Supplementary Notes For more information write to address in block 9.		

16 Abstract

Lightweight Cellular Concrete (LCC) (also called foam or gas concrete) is a special construction material, which is typically composed of portland cement, water, and air voids created by a foaming agent. This material has been increasingly used as a backfill material for geotechnical applications. This report presents a series of laboratory tests conducted to evaluate the material properties of LCC including density, permeability, compressive strength, shear strength, compressibility, elastic modulus, and Poisson's ratio with different cement to fly ash ratios and at different ages. LCC specimens used in this research project were cast in the field, and the cement to fly ash ratios used for the production of the specimens ranged from 50:50 to 100:0. Large direct shear box tests were conducted on prismatic specimens with a size of 12 inches long, 12 inches wide, and 8 inches high, while small direct shear box tests were conducted on cylindrical specimens with a size of 2.5 inches in diameter and 1 inch high. This report also presents a series of pullout tests conducted in the laboratory to investigate pullout resistance of extensible reinforcement (geogrid) and inextensible reinforcement (steel strip) embedded in LCC. Pullout displacements and pullout forces were monitored using linear variable displacement transducers (LVDT) and a load cell during the pullout process. This research project investigated the effects of age, normal stress, LCC type, cold joint, and re-pullout on pullout resistance and calculated the pullout resistance factors F* for geogrid and steel strip embedded in LCC.

The laboratory material test results show that the average wet densities of LCC ranged from 30 to 36 pcf at the age of 28 days and the average dry densities ranged from 21 to 24 pcf at the same age. The permeability values of LCC ranged from 2.1×10-5 to 3.0×10-4 in./s and they increased as the cement to fly ash ratio increased. The measured cohesion values of LCC in large direct shear box tests ranged from 33 to 50 psi, while the measured cohesion values in small direct shear box tests ranged from 19 to 37 psi. This report also compares the material properties of LCC measured in this research project with those reported in the literature and shows overall good agreement.

The laboratory pullout test results show that for the geogrid embedded in LCC, the maximum pullout force increased as the normal stress increased. For the steel strip embedded in LCC, the maximum pullout force was independent of the normal stress and increased as the age and the cement to fly ash ratio increased. Pullout test results also show that the presence of a cold joint did not reduce the pullout resistance, while the re-pullout test had lower pullout resistance as compared with the original pullout test for the same specimen. The pullout resistance factors F* for steel strips were greater than those for geogrids and these factors decreased as the normal stress increased.

17 Key Words Reinforcement, Air Voids, Backfilling, Foaming Agents, Geogrids		**18 Distribution Statement** No restrictions. This document is available to the public through the National Technical Information Service www.ntis.gov.	
19 Security Classification (of this report) Unclassified	**20 Security Classification (of this page)** Unclassified	**21 No. of pages** 87	**22 Price**

Form DOT F 1700.7 (8-72)

This page intentionally left blank.

Pullout Resistance of Reinforcement of Lightweight Cellular Concrete Fill

Final Report

Prepared by

Jie Han, Ph.D., P.E., F.ASCE
Yuqiu Ye, M.S.
Robert L. Parsons, Ph.D., P.E.
Matt O'Reilly, Ph.D., P.E.
Hao Liu, Ph.D.

The University of Kansas

A Report on Research Sponsored by

THE KANSAS DEPARTMENT OF TRANSPORTATION
TOPEKA, KANSAS

and

THE UNIVERSITY OF KANSAS
LAWRENCE, KANSAS

August 2023

PREFACE

The Kansas Department of Transportation's (KDOT) Kansas Transportation Research and New-Developments (K-TRAN) Research Program funded this research project. It is an ongoing, cooperative and comprehensive research program addressing transportation needs of the state of Kansas utilizing academic and research resources from KDOT, Kansas State University and the University of Kansas. Transportation professionals in KDOT and the universities jointly develop the projects included in the research program.

NOTICE

The authors and the state of Kansas do not endorse products or manufacturers. Trade and manufacturers names appear herein solely because they are considered essential to the object of this report.

This information is available in alternative accessible formats. To obtain an alternative format, contact the Office of Public Affairs, Kansas Department of Transportation, 700 SW Harrison, 2nd Floor – West Wing, Topeka, Kansas 66603-3745 or phone (785) 296-3585 (Voice) (TDD).

DISCLAIMER

The contents of this report reflect the views of the authors who are responsible for the facts and accuracy of the data presented herein. The contents do not necessarily reflect the views or the policies of the state of Kansas. This report does not constitute a standard, specification or regulation.

Abstract

Lightweight Cellular Concrete (LCC) (also called foam or gas concrete) is a special construction material, which is typically composed of portland cement, water, and air voids created by a foaming agent. This material has been increasingly used as a backfill material for geotechnical applications. This report presents a series of laboratory tests conducted to evaluate the material properties of LCC including density, permeability, compressive strength, shear strength, compressibility, elastic modulus, and Poisson's ratio with different cement to fly ash ratios and at different ages. LCC specimens used in this research project were cast in the field, and the cement to fly ash ratios used for the production of the specimens ranged from 50:50 to 100:0. Large direct shear box tests were conducted on prismatic specimens with a size of 12 inches long, 12 inches wide, and 8 inches high, while small direct shear box tests were conducted on cylindrical specimens with a size of 2.5 inches in diameter and 1 inch high. This report also presents a series of pullout tests conducted in the laboratory to investigate pullout resistance of extensible reinforcement (geogrid) and inextensible reinforcement (steel strip) embedded in LCC. Pullout displacements and pullout forces were monitored using linear variable displacement transducers (LVDT) and a load cell during the pullout process. This research project investigated the effects of age, normal stress, LCC type, cold joint, and re-pullout on pullout resistance and calculated the pullout resistance factors F^* for geogrid and steel strip embedded in LCC.

The laboratory material test results show that the average wet densities of LCC ranged from 30 to 36 pcf at the age of 28 days and the average dry densities ranged from 21 to 24 pcf at the same age. The permeability values of LCC ranged from 2.1×10^{-5} to 3.0×10^{-4} in./s and they increased as the cement to fly ash ratio increased. The measured cohesion values of LCC in large direct shear box tests ranged from 33 to 50 psi, while the measured cohesion values in small direct shear box tests ranged from 19 to 37 psi. This report also compares the material properties of LCC measured in this research project with those reported in the literature and shows overall good agreement.

The laboratory pullout test results show that for the geogrid embedded in LCC, the maximum pullout force increased as the normal stress increased. For the steel strip embedded in LCC, the maximum pullout force was independent of the normal stress and increased as the age and the cement to fly ash ratio increased. Pullout test results also show that the presence of a cold joint did not reduce the pullout resistance, while the re-pullout test had lower pullout resistance as compared with the original pullout test for the same specimen. The pullout resistance factors F^* for steel strips were greater than those for geogrids and these factors decreased as the normal stress increased.

Acknowledgments

This research project was jointly supported by the Kansas Department of Transportation through the K-TRAN program and the Cematrix Corp. The authors thank Mr. Luke Metheny, the project monitor and KDOT Chief Geotechnical Engineer, Mr. James Brennan, the former KDOT Chief Geotechnical Engineer, Mr. Brad Dolton, the manager of geotechnical solutions for Cematrix, and Mr. Stephen Rachford, an independent consultant, for their guidance and support. Technician, Kent Dye, from the Civil, Environmental & Architectural Engineering (CEAE) Department at the University of Kansas provided his assistance in modifying the pullout box. All the above support and assistance are greatly appreciated.

Table of Contents

List of Tables

List of Figures

Chapter 1: Introduction

1.1 Background and Problem Statement

Lightweight Cellular Concrete (LCC) (also called foam concrete or gas concrete) has favorable material properties, such as low self-weight, high compressive strength, low or high permeability, good thermal insulation, and good fire resistance. LCC was initially used in small-scale projects due to the lack of effective foaming agents and production equipment. Over the past 30 years, the improvement of production equipment, foam agents, and binders enhanced the applications of LCC in large-scale projects. However, the type of binder, the method of foaming, the use of other ingredients (e.g., fly ash), and the curing condition all have significant influences on the properties of LCC. The effect of fly ash on the properties of LCC has not been well evaluated. Therefore, it is important to study the effect of fly ash on the material properties of LCC. For LCC as a cementitious material, age plays an important role in its properties and therefore should be evaluated as well.

LCC has been increasingly used as a backfill in geotechnical applications including mechanically stabilized earth (MSE) walls. However, there have been limited studies on the pullout resistance of geosynthetic or steel reinforcement embedded in LCC. Ramezani, Vilches, and Neitzert (2013) conducted small-scale model tests and numerical simulations to investigate the pullout resistance of steel strips embedded in LCC with different reinforcement geometries and patterns. Their pullout tests consisted of a galvanized steel strip (2 inches wide × 3 inches long) cast in the middle of a foam concrete cube (4 inches × 4 inches × 4 inches). Their test results revealed that the interface (bonding) strength between the steel strip and the LCC was mainly provided by chemical adhesion, which depended on the age. Their investigation was mainly for structural applications and the density of the LCC was 75 pcf, which is almost double that used for geotechnical applications. To the best knowledge of the authors, so far, no publication is available in the literature about pullout resistance of geosynthetics in LCC. Therefore, research is needed to evaluate the pullout behavior of reinforcement in LCC, especially geosynthetic reinforcement in LCC.

Past studies on the properties of LCC have been conducted based on specimens prepared in the laboratory. These specimens may not represent well the behavior of LCC cast in the field. Therefore, it is necessary to evaluate LCC specimens cast under field conditions.

1.2 Objective

The main objectives of this research were:

1. To understand the state of the practice on the material properties of LCC and its geotechnical applications;
2. To evaluate the material properties of LCC cast in the field with different cement to fly ash ratios and at different ages; and
3. To evaluate the pullout resistance of geogrid and steel strip embedded in LCC with different cement to fly ash ratios and at different normal stresses and ages and calculate their corresponding pullout resistance factors F^*.

1.3 Research Methodology

This study adopted the following research methodologies:

1. A literature review to summarize the state of the practice on LCC composition (e.g., binder, other ingredients, and foam agent), material properties (e.g., density, permeability, compressive and shear strengths, modulus of elasticity, thermal conductivity, and fire resistance), its geotechnical applications (e.g., foundation and backfill, pavement base and geotechnical fill), and the pullout resistance of reinforcement embedded in different materials;
2. Laboratory tests to evaluate the material properties of LCC including density, permeability, compressive strength, shear strength, compressibility, elastic modulus, and Poisson's ratio with different cement to fly ash ratios and at different ages; and

3. Laboratory pullout tests to evaluate the pullout resistance of extensible (geogrid) and inextensible (steel strip) reinforcement embedded in LCC with different cement to fly ash ratios and at different normal stresses and different ages.

All the specimens tested in the laboratory were cast on one field project. The LCC mix with the cement to fly ash ratio of 75:25 was used for the field project. For the research purpose, two other mixes with the cement to fly ash ratios of 50:50 and 100:0 were also cast on the field project. During the production of the LCC 50:50 mix, insufficient water was added due to an operational error; therefore, these specimens are not representative and excluded in this report. To replace this mix, the second mix for LCC 50:50 specimens was produced onsite. Unfortunately, only one large direct shear box and no pullout box were available for the second mix of LCC 50:50 specimens. Therefore, this report only includes the available test results on the second mix of LCC 50:50 specimens.

1.4 Report Organization

This report consists of five chapters. Chapter 1 presents an introduction including background and problem statements, objectives, research methodology, and organization of the report. Chapter 2 presents the literature review on the LCC composition, material properties, its geotechnical applications, and the pullout resistance. Chapter 3 presents the laboratory tests on the material properties of LCC. Chapter 4 presents the laboratory pullout tests on geogrid and steel strip in LCC and the calculated pullout resistance factors F^*. Chapter 5 presents the conclusions and recommendations from this research.

Chapter 2: Literature Review

Lightweight Cellular Concrete (LCC) (also named foam concrete or gas concrete) is a special construction material, which typically consists of portland cement, water, and air voids created by a foaming agent. This material has been increasingly used as a backfill material for geotechnical applications in recent years. Researchers and engineers have performed laboratory tests, model tests, and field tests to study its material properties and field performance. To have a better understanding of the LCC properties, this chapter summarizes and assesses the material composition (e.g., binder, other ingredients, and foam agent) and the properties (e.g., density, permeability, compressive and shear strengths, modulus of elasticity, thermal conductivity, and fire resistance). This section also provides a brief review of its geotechnical applications as a backfill material for mechanically stabilized earth walls, foundations, road bases, and void filling, and the performance of reinforcement embedded in different materials under pullout conditions.

2.1 LCC composition

2.1.1 Air Voids

Air voids are one of the controlling factors in the production of LCC. Narayanan and Ramamurthy (2000) summarized two methods to create air voids: (1) gas-forming chemicals mixed with a cement mortar during a liquid or plastic stage to increase the volume (i.e., air voids are generated while gas escapes) and (2) foam pre-created using foaming agents mixed with a cement mortar (no chemical reaction involved thus recognized as an economical and controllable method to create air voids).

2.1.2 Binder

The most commonly used binder for LCC is cement, typically portland cement. To reduce costs and protect the environment, the construction industry has been looking for alternate cement. Calcium aluminate cement, calcium sulfoaluminate cement, alkali-activated binder, and supersulfated cement have all been considered alternatives to portland cement (Juenger, Winnefeld, Provis, & Ideker, 2011). Fly ash, slag, silica fume, pulverized fuel ash, and slate waste

have also sometimes been used as partial replacements for cement. However, the high content of fly ash may reduce the strength and increase the time required to reach the ultimate strength (Liu et al., 2020; Kearsley & Wainwright, 2001).

2.1.3 Other Ingredients

To achieve the desired strength at a low cost, quartz sand and soil have been adopted as a replacement for fly ash in the production of LCC (Ma & Chen 2015; Yang & Chen, 2016). Carbon nanotubes have also been used as an ingredient by Yakovlev, Kerienė, Gailius, and Girnienė (2006) and they found a more homogenous cell structure with closed air voids when carbon nanotubes were used. Moreover, the addition of other ingredients has a significant influence on the density of LCC as heavier ingredients result in higher density.

2.1.4 Foaming Agent

Commonly used foaming agents include natural foaming agents and synthetic foaming agents. Natural foaming agents have a limited storage life and their properties have great variation, while synthetic foaming agents have a long storage life and stable properties. Therefore, synthetic foaming agents have been increasingly used in industry. The content of the foaming agent has a considerable effect on the material properties of both fresh and hardened LCC. An excessive foam volume may cause a decrease in flowability during the production of LCC.

2.1.5 Water

LCC is more sensitive to water demand than normal-weight concrete. If too little water is added to a mixture, water may not be sufficient for the initial reaction of cement so that the cement will withdraw water from the foam, causing rapid degeneration of the foam. If too much water is added, segregation may take place and cause a variation in density. Ramamurthy, Nambiar, and Ranjani (2009) proposed that the typical water to cement ratio for the production of LCC should range from 0.4 to 1.25. To prevent cement from taking water from the foam, Kearsley and Mostert (2005) suggested the minimum water to cement ratio should be 0.35. In the production of high-density LCC (87 to 112 pcf), the typical water to cement ratio ranges from 0.35 to 0.5 (Jones & McCarthy, 2005b).

2.2 LCC properties

2.2.1 Density

Typical wet densities of LCC range from 24 to 50 pcf. For the applications below the ground, Ni, Oyeyi, and Tighe (2020) suggested the range of wet densities should be from 25 to 37 pcf. Based on the density variation, Ozlutas (2015) classified LCC as: (1) ultra-low density cellular concrete (below 37 pcf), (2) low-density cellular concrete (37 to 62 pcf), and (3) high-density cellular concrete (above 62 pcf). Density of fresh cast LCC is 15–25% heavier than dry density and this percentage can be as high as 45% for low-density LCC (Narayanan & Ramamurthy, 2000). Cement, other ingredients, and porosity (air voids) are the main factors influencing the density. Material properties, such as the modulus of elasticity, compressive strength, and thermal resistance, can be indirectly quantified with their density.

2.2.2 Compressive Strength

Narayanan and Ramamurthy (2000) summarized typical compressive strength values for LCC with different densities, which are shown in Table 2.1. Compressive strength is reported to increase as the density increases and the porosity decreases (Ramamurthy et al., 2009; Narayanan & Ramamurthy, 2000). Water to cement ratio, foaming agent, other ingredients, and curing condition have significant influences on compressive strengths. Narayanan and Ramamurthy (2000) pointed out that for a given density, LCC with fine materials has higher compressive strength than LCC with coarse materials because LCC with fine materials has a comparatively uniform distribution of air voids, while larger and irregular air voids exist in mixes with coarse materials. Rao, Zhang, Ye, Liu, and Han (2021) found that foamed concrete had larger coefficients of variation in the strength and modulus than in the density in the same group due to their differences in void structures.

2.2.3 Modulus of Elasticity

The modulus of elasticity of LCC is significantly lower than that of normal-weight concrete. For LCC with densities ranging from 31 to 94 pcf, the typical modulus of elasticity ranges from 145 to 1,160 ksi (Ramamurthy et al., 2009). The LCC with sand had a higher modulus of elasticity than that with fly ash (Jones, 2001), and the use of polypropylene fibers increased the

modulus of elasticity up to four times (Jones & McCarthy, 2005b). The modulus of elasticity of LCC has a relationship with its compressive strength and density. Table 2.2 shows the formulas for estimating the modulus of elasticity summarized by Narayanan and Ramamurthy (2000). In addition, a stress-strain curve obtained from a compression test of LCC can be used to determine its modulus of elasticity.

Table 2.1: Compressive strengths of LCC at different densities

Dry density (pcf)	Compressive strength (psi)	Modulus of elasticity (ksi)
25	188–406	26–170
31	290–638	180–267
37	406–914	255–383
44	565–1233	351–519

Source: Narayanan and Ramamurthy (2000)

Table 2.2: Formulas for estimating the elastic modulus of LCC

Reference	Equation	Remark
Tada (1986)	$E = 5.31W - 853$	Density from 200 to 800 kg/m^3
McCormick (1967)	$E = 33W^{1.5}\sqrt{f_c}$	Pauw's equation
Jones and McCarthy (2005b)	$E = 0.42 f_c^{1.18}$	Sand as an ingredient
	$E = 0.99 f_c^{0.67}$	Fly ash as an ingredient

Notes: W is the density in kg/m^3, f_c is the compressive strength in GPa, and E is the modulus of elasticity in GPa.
Source: Ramamurthy et al. (2009)

2.2.4 Poisson's Ratio

Poisson's ratio is defined as the ratio of transverse strain to axial strain for a specimen subjected to an axial load and it is one of the most important parameters to determine the stress, strain, and displacement (TAC, 2013). Ni et al. (2020) summarized Poisson's ratios of LCC available in the literature. Laboratory tests in Tiwari et al. (2017) showed that for LCC specimens

with densities from 19 to 48 pcf, the measured Poisson's ratios were in the range of 0.2 to 0.3. Lee, Hardy, and Bronowski (2004) found that for LCC with densities of 62 pcf and 87 pcf, the measured Poisson's ratios ranged from 0.13 to 0.16 and 0.18 to 0.19, respectively, indicating that the higher density LCC had the lower Poisson's ratio.

2.2.5 Friction Angle and Cohesion

Direct shear tests in Tiwari et al. (2017) showed that the measured effective friction angle and cohesion were 35° and 5 psi, respectively. The commonly-used backfill (i.e., granular materials) for MSE walls is cohesionless. Tiwari et al. (2017) suggested using an effective friction angle of 35° and ignoring the cohesion for LCC as the backfill in the design of MSE walls. So far, there are limited investigations on the friction angle and cohesion for LCC, but they deserve further investigations because they are important parameters for the design of MSE walls with LCC as the backfill. Tiwari et al. (2017) conducted small direct shear tests on LCC specimens with cement as a binder and obtained the following empirical relationships between the friction angle and cohesion of LCC and its unit weight:

$$\varphi = 1.1\gamma + 15.1$$

Equation 2.1

$$c = 274.4\gamma - 655.0$$

Equation 2.2

Where: γ is the unit weight in kN/m^3, φ is the friction angle in degree, and c is the cohesion in kPa.

2.2.6 Permeability

Soil Exploration Company (1981) reported the permeability of LCC was in the order of 10^{-7} in./s. Laboratory test results from Tiwari et al. (2017) showed that the measured permeability values ranged from 6.7×10^{-5} to 4.7×10^{-4} in./s. Typical permeability values for gravel, clean sand, very fine to fine sand, and homogeneous clay were in the range of 0.4 to 2.0, 10^{-3} to 10^{-2}, 10^{-4} to

10^{-3}, and 10^{-9} to 10^{-7} in./s respectively. Therefore, the permeability values of LCC are lower than those of gravel, clean sand, and very fine to fine sand, but higher than those of homogeneous clays.

2.2.7 Thermal Conductivity/Insulation

For LCC with dry densities from 37 to 100 pcf, typical thermal conductivity values ranged from 0.1 to 0.7 W/mK (Jones & McCarthy, 2005a). Thermal conductivity of LCC depends on density, moisture content, and ingredients of the material, and can be expressed as a function of density (Narayanan & Ramamurthy, 2000). Moreover, the number of air voids and their distribution are critical to the performance of thermal insulation. Narayanan and Ramamurthy (2000) pointed out that LCC with finer pores had better thermal insulation. Tada (1986) proposed an LCC design guideline for buildings with a requirement for thermal insulation. Lim, Tan, Lim, and Lee (2013) conducted a series of laboratory tests to investigate the influence of oil fuel as a filler on the thermal properties of LCC. Their test results indicated that densification of microstructures in LCC slightly increased the thermal conductivity.

2.2.8 Fire Resistance

Heat transfer in porous materials mainly depends on radiation that is an inverse function of air-solid interfaces (Ramamurthy et al., 2009). LCC has better fire resistance than normal-weight concrete. As LCC has a large number of air voids, heat transfer can be significantly inhibited, which makes LCC an ideal fire resistance material. Fire resistance tests showed that a decrease in LCC density increased its fire endurance (Ramamurthy et al., 2009). Aldridge (2005) reported that a low-density LCC exhibited better fire resistance than a high-density LCC due to more air voids inside.

2.3 LCC Applications

LCC has been increasingly used in geotechnical projects due to its versatility and advantages. Mohd and Mohammed (2017) classified the applications of LCC in geotechnical projects according to its density.

2.3.1 Foundation and Backfill

LCC with a density ranging from 19 to 37 pcf is recommended for foundation soil and backfill because its light self-weight imposes low vertical stresses on subsoils (Jalal, Tanveer, Jagdeesh, & Ahmed, 2017). Hulimka, Krzywoń, and Knoppik-Wróbel (2011) listed the advantages of using LCC to replace compacted soil as a foundation soil including: (1) desired strength; (2) easy pouring and limited settlement; and (3) no compaction needed. Tian, Li, Zhao, Zhou, and Wang (2009) reported the use of LCC as a backfill material for bridge abutments in Guangzhou, China, which reduced the applied load and the settlement of the soft foundation below the abutment. Watabe and Noguchi (2011) reported the use of LCC as a retaining wall backfill in Tokyo, Japan, to reduce the stress on the foundation soil.

2.3.2 Pavement Subbase

LCC with a density ranging from 31 to 37 pcf is recommended for its application for pavement subbases. LCC was first used as a road subbase material in Canada in 2000 (Panesar, 2013) and later used in Holland (Mindess, 2019). Ni et al. (2020) summarized the advantages of LCC used for pavement subbases including (1) low cost at repair and rehabilitation, (2) less settlement, and (3) good resistance to freeze-thaw and frost heave. As compared with commonly-used road subbase materials (i.e., dense sand and gravel with fines), LCC is less susceptible to freeze and thaw. Ni et al. (2020) presented three projects in Canada, in which LCC was used as subbases in pavements: (1) LCC with the density of 30 pcf used as the subbase for roadways and sidewalks in Victoria, British Columbia (significantly improved the performance and durability of pavements), (2) LCC used as a replacement for the peat material in the rural road in Region of Peel in Ontario (reduced the fill weight and the environmental impact on the connecting wetlands), and (3) LCC used as a subbase to reconstruct bus lanes in Calgary, Alberta (solved the problems of frost-heave). The AASHTO (1993) guideline for flexible pavement and rigid pavement design was developed based on sand and gravel subbases. However, there is no well-accepted design guideline available to date for pavement design with LCC as a subbase.

2.3.3 Geotechnical Fill

LCC with a density ranging from 37 to 50 pcf is recommended for geotechnical fill. It has been increasingly used as an alternative to granular materials in the void filling, such as filling of space around pipes, walls, basements, and subways. Freshly-cast LCC is extremely flowable so that it can easily fill tiny voids even without removing underground structures, which provides an economical and simple solution for abandoned tunnels, underground tanks, and naturally occurring voids. Tian et al. (2009) reported LCC was used to fill the gap between a pipe and a tunnel in Shanxi, China. Jalal et al. (2017) reported the use of LCC to fill disused fuel tanks in London, UK, to replace the removed original fill in South Dakota, USA, to reduce settlement and protect an existing bridge structure, and to fill a network of six pedestrian subways in Milton Keynes, UK.

2.4 Pullout Resistance

Pullout resistance of reinforcement in soil mainly depends on the frictional resistance of longitudinal bars and the bearing resistance of transversal bars (Bergado & Chai, 1994; Alfaro, Hayashi, Miura, & Watanabe, 1995; Tran, Meguid, & Chouinard, 2013; Moraci et al., 2014). Palmeira and Milligan (1989) evaluated scale and other factors affecting the results of pull-out tests of grid buried in sand. Based on experimental tests, Esfandiari and Selamat (2012) established an empirical formula for predicting the pullout resistance of steel strips embedded in soil considering the effect of transverse bars. Sukmak et al. (2015) investigated the effect of fine content on the pullout resistance mechanism of bearing reinforcement embedded in cohesive-frictional soils. Morsy, Zornberg, Han, and Leshchinsky (2019) developed a new pullout device to investigate geosynthetic-soil interaction using active and boundary reinforcements in the test setup.

FHWA (Berg, Samtani, & Christopher, 2009), CGS (2006), AASHTO (2012), and Moraci et al. (2014) provided the formulae for calculating the pullout capacity of reinforcement embedded in soil for embankments, slopes, and retaining walls. Among these formulae, FHWA (Berg et al., 2009) provided the most commonly used equation as follows:

$$P = C \cdot F^* \cdot \alpha \cdot \sigma_v \cdot L_e$$

Equation 2.3

Where: P is the ultimate pullout resistance per unit width, C is the overall reinforcement surface area geometry factor based on the gross perimeter of the reinforcement (equal to 2 for strip, grid, and sheet-type reinforcements), F^* is the pullout resistance factor, α is a scale effect correction factor (1.0 for metal reinforcement and 0.6 to 1.0 for geosynthetic reinforcements), σ_v is the normal stress at the reinforcement level, and L_e is the embedment length. FHWA (Berg et al., 2009) suggested a typical value of α = 0.8 for geogrids.

Past studies have also investigated the pullout behavior of steel or polymer reinforcement embedded in normal-weight concrete. For example, Ben-Romdhane and Ulm (2002) proposed a theoretical model for calculating the interface shear stresses between steel bars and concrete. Bouazaoui and Li (2008) evaluated the interface shear strength between steel bars and concrete using pullout tests and proposed an analytical model for estimating this shear strength. Baena, Torres, Turon, and Barris (2009) conducted a series of pullout tests on carbon-fiber and glass-fiber-reinforced polymers embedded in normal-weight concrete and found that concrete with a higher strength led to higher interface shear strength between the polymer and concrete. Ramezani et al. (2013) pointed out that the pullout resistance of a steel strip embedded in concrete mainly depended on chemical bonding, friction resistance, and bearing resistance (mechanical interlock). The chemical bonding strength between the steel surface and the surrounding concrete was first mobilized under the initial pullout load. After the chemical bonding broke, the friction and bearing resistances developed and the relative displacement between the steel strip and concrete occurred.

Chapter 3: Laboratory Material Tests

This chapter presents a series of laboratory tests conducted to evaluate the material properties of LCC including density, permeability, compressive strength, shear strength, elastic modulus, Poisson's ratio, and compressibility with different cement to fly ash ratios and at different ages. LCC specimens used in this study were cast in the field at the cement to fly ash ratios of 50:50, 75:25, and 100:0. Large direct shear box tests consisted of prismatic dimensions of 12 inches long, 12 inches wide, and 8 inches high, while small direct shear box tests consisted of cylindrical dimensions of 2.5 inches in diameter and 1 inch high.

3.1 Laboratory Test Methods

3.1.1 Specimen Preparation

LCC specimens used in this study were cast in the field during the installation of LCC as a backfill material for a mechanically stabilized earth wall in Kansas City, Kansas. The LCC was composed of portland cement, fly ash (for some mixes), water, and air voids created by foam agents. The mixtures adopted the foaming method to generate air voids. Specifically, foams were pre-formed by mixing the foam agents with water under a high-pressure condition, and then foams were mixed with cement and fly ash slurry in a special chamber. The specimens of LCC were cast in molds in the field, left on the site overnight, and then transported to the laboratory for curing in a temperature-controlled and moisture-controlled environment according to ASTM C511-21 (2021). Specimens were demolded upon arrival at the laboratory except for some LCC (50:50) specimens, which did not have sufficient strength for demolding until 7 days. To investigate the influence of the cement to fly ash ratio on the properties of LCC, specimens were created from mixtures with three cement to fly ash ratios of 50:50, 75:25, and 100:0. Ramamurthy et al. (2009) reported typical water to cement ratios for the production of LCC ranging from 0.4 to 1.25. This study adopted water to cement ratio of 0.55, which was within the range of their recommendations. LCC (75:25) specimens were cast on four consecutive days to evaluate the variability of the mixtures since this mix was used for the field project. For easy presentation, LCC (75:25)

specimens cast on different days are indicated with -a, -b, -c, and -d. Table 3.1 shows the collected information about the LCC specimens.

Table 3.1: Collected information about the LCC specimens

Specimen type	Water to cement ratio	Cement to fly ash ratio	Cast day
LCC (50:50)	0.55	50:50	Oct. 01, 2020
LCC (75:25)-a	0.55	75:25	Sept. 28, 2020
LCC (75:25)-b	0.55	75:25	Sept. 29, 2020
LCC (75:25)-c	0.55	75:25	Sept. 30, 2020
LCC (75:25)-d	0.55	75:25	Oct. 01, 2020
LCC (100:0)	0.55	100:0	Oct. 01, 2020

3.1.2 Density Test

Wet density and dry density of LCC specimens were measured at ages of 3 or 4, 7, 14, 28, and 56 days after casting. The specimens used for the measurement of density had a nominal diameter of 3 inches and a height of 6 inches. The wet density was measured immediately upon removal from the curing room and after removal of any standing surface water, while the dry density was measured after the demolded specimen was left in the oven for at least 24 hours.

3.1.3 Permeability Test

Permeability tests for LCC specimens were conducted using a flexible wall permeameter (i.e., inside the triaxial cell) using Method C (a falling head method) following ASTM D5084-10 (ASTM, 2010) at the age of 180 days. The specimens used for the permeability tests had a nominal diameter of 2.75 inches and a height of 5.5 inches, and were trimmed from the cast specimens that had a nominal diameter of 3 inches and a height of 6 inches. The hydraulic gradients used for these tests ranged from 1.0 to 5.5. The confining pressures of 2, 4.5, and 9 psi were selected to ensure the membrane was in good contact with the specimen. Each specimen was saturated by increasing the cell pressure and simultaneously applying a back-pressure. Saturation was verified by

measuring the pore water *B* value, and the test specimen was considered fully saturated when the *B* value was greater than 0.95.

3.1.4 Unconfined Compression Test

Unconfined compression tests were conducted at the ages of 3 or 4, 7, 14, 28, and 56 days following a modified version of ASTM C39-21 (2021). The specimens used for the unconfined compression tests had a nominal diameter of 3 inches and a height of 6 inches. Specimens were sulfur capped on both ends before testing. The typical stress rate for the unconfined compression test on normal-weight concrete was 34 psi/s. Considering the relatively low strength of LCC, a stress rate of 10 psi/s was selected in the unconfined compression test for LCC. The compression test was performed at the selected stress rate until the peak strength value was reached.

3.1.5 Direct Shear Test

The direct shear tests for LCC were conducted at the age of 28 days following ASTM D3080-11 (2011). The influence of the specimen size on its shear strength was investigated using both large and small specimens. The large specimens were 12 inches long, 12 inches wide, and 8 inches high, while the small specimens are 2.5 inches in diameter and 1 inch in height. Tiwari et al. (2017) adopted a shear displacement rate of 0.004 in./min in their laboratory direct shear tests on LCC and obtained good test results. Therefore, this study selected the same shear rate of 0.004 in./min for all the direct shear tests. To investigate the influence of overburden stresses on shear strengths of LCC in typical applications, the selected normal stresses ranged from 1.5 to 9 psi for direct shear tests. The measured peak shear force for LCC (50:50) at the normal stress of 4.5 psi in the large direct shear test almost reached the capacity of the load cell. Evidence shows that an LCC with a higher cement to fly ash ratio would have a higher shear strength. Therefore, to protect the large direct shear test device, the maximum normal stresses for LCC (75:25) and LCC (100:0) were reduced to 4.5 psi. The specimen was sheared at the selected shear displacement rate until passing the peak shear stress.

3.1.6 Elastic Modulus and Poisson's Ratio Test

Modulus of elasticity and Poisson's ratio of LCC were determined at the age of 56 days following a modified ASTM C39 (2015). The specimens used for the Poisson's ratio and modulus of elasticity tests had a nominal diameter of 3 inches and a height of 6 inches. Strain gauges were placed on the mid-height of each specimen in the vertical and circumferential directions. A load was applied to the specimen and increased until it failed. Specimens were loaded in a manner identical to the unconfined compression tests. The elastic modulus of each specimen was calculated as the slope of the stress-strain curve in the region of strains between 10% and 45%. This approach is commonly used to estimate the elastic modulus of concrete and is similar to the method for the elastic modulus of soil-cement, E_{50} (the slope of the stress-strain curve in the region of strains between 0% and 50%) (Han, 2015). The reported elastic modulus and Poisson's ratio values in this report were the average values from two samples for the same type of LCC.

3.1.7 One-Dimensional Consolidation Test

One-dimensional consolidation tests were performed to evaluate the consolidation properties of LCC at the age of 180 days, such as the compression index, the recompression index, and the coefficient of consolidation following Method A in ASTM D2435/D2435M-11 (2011). The deformation of an LCC specimen under loading was monitored using LVDT. The cylindrical specimens cast in the field were trimmed into a suitable dimension of 2.4 inches in diameter and 0.8 inches in height for the consolidation tests. After the trim was finished, the specimens were placed in a water tank to be saturated.

3.2 Test Results and Discussion

3.2.1 Density

Figure 3.1 shows the measured wet and dry density values of LCC versus the age for LCC specimens cast in the field. The density value for each mix at each age was calculated as an average from three or four specimens. ACI (2006) classified LCC as Classes I, II, III, IV, V, and VI based on the maximum cast density. Figure 3.1 includes the lines corresponding to the LCC classification based on ACI (2006). In general, the measured wet densities of LCC specimens were in the range

of Classes II to IV except for LCC (75:25)-d, while most measured dry densities of LCC in this study were lower than those of Class II LCC except LCC (75:25)-d.

Figure 3.2 shows the average wet and dry density values of LCC at each mix versus age for further analysis. LCC (50:50) and LCC (100:0) had one mix each so their average density values were those for their mixes. Since LCC (75:25)-d is considered as an outlier, the average density values of LCC (75:25) were calculated based on LCC (75:25)-a, LCC (75:25)-b, and LCC (75:25)-c. For comparison, Figure 3.2 includes the reference line of water density. For LCC (50:50), LCC (75:25), and LCC (100:0) at the age of 28 days, the average dry densities were 22, 24, and 21 pcf, and the average wet densities were 30, 36, and 34 pcf, respectively at the same age. In other words, the dry density was approximately 67% of the wet density. The LCC densities measured in this study were consistent with those reported by Narayanan and Ramamurthy (2000), but slightly lower than those obtained by Tiwari et al. (2017). Figure 3.2 clearly shows that all the LCC density values were lower than that of water due to the existence of a large volume of air voids inside the specimens. Based on the Ozlutas (2015) classification, the LCC utilized in this study was an ultra-low density cellular concrete. Since the measured wet densities of LCC (100:0) had large variations, a trend line based on a two-order logarithmic function is included in Figure 3.2a. The wet density of LCC (100:0) used for the calculation of elastic modulus later in the report was determined based on this trendline.

3.2.2 Permeability

Figure 3.3 shows the variations of the measured permeability with the hydraulic gradient for LCC subjected to confining stresses of 2, 4.5, and 9 psi. LCC (50:50), LCC (75:25)-b, and LCC (100:0) specimens were used for permeability tests. In general, the permeability decreased as the hydraulic gradient increased because a higher hydraulic gradient might induce turbulent flow. In addition, the permeability decreased generally as the confining stress increased. The increase of the confining stress compressed the LCC specimen and reduced the sizes of voids, thus resulting in a reduction of the measured permeability. For LCC (50:50), LCC (75:25)-b, and LCC (100:0), the measured permeability values ranged from 2.1×10^{-5} to 6.7×10^{-5}, 3.1×10^{-5} to 7.3×10^{-5}, and 1.9×10^{-4} to 3.0×10^{-4} in./s, respectively, indicating that the LCC with a higher cement to fly ash

ratio had higher permeability. In other words, fly ash reduced the permeability of LCC. Tiwari et al. (2017) reported a measured permeability of 6.7×10^{-5} to 4.7×10^{-4} in./s for LCC (100:0) with a wet density of 19 to 48 pcf, which was higher than those measured in this study as shown in Table 3.2. The measured permeability from both Tiwari et al. (2017) and this study was higher than that reported by Soil Exploration Company (1981). Gravel and clean sand are commonly used backfill materials. The typical permeability values for gravel and clean sand were in the range of 0.4 to 2 and 10^{-3} to 10^{-2} in./s. The permeability values of LCC measured in this study are lower than those of gravel and clean sand.

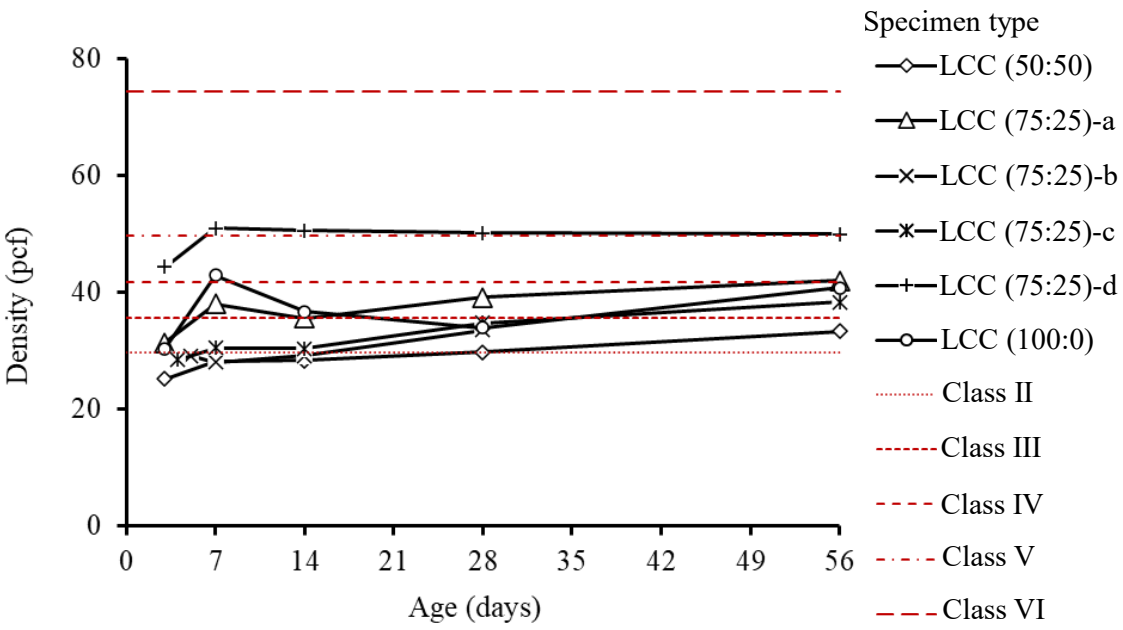

(a) Wet Density

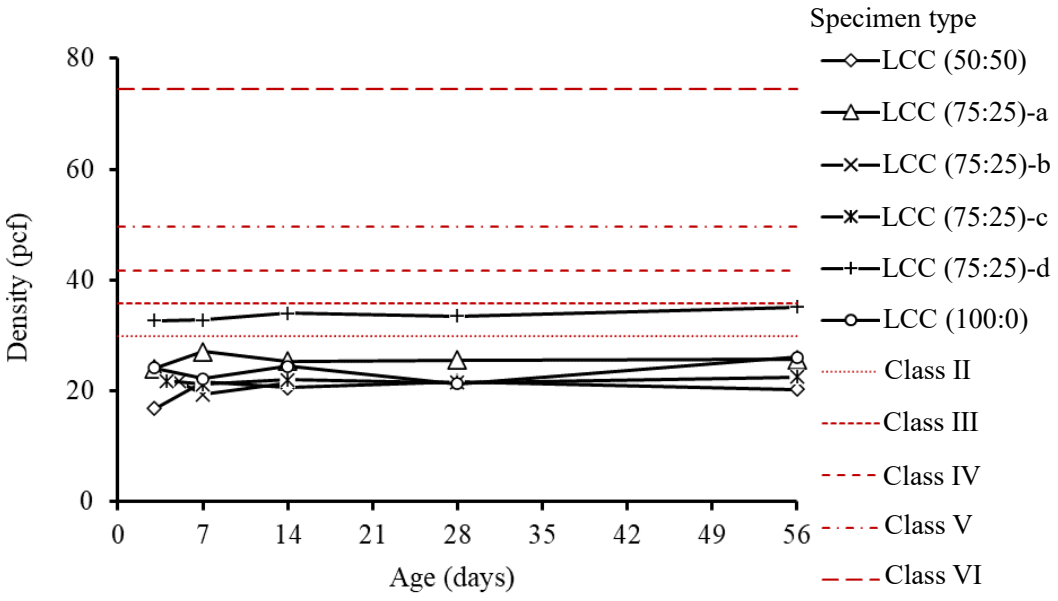

(b) Dry Density

Figure 3.1: Density Versus Age

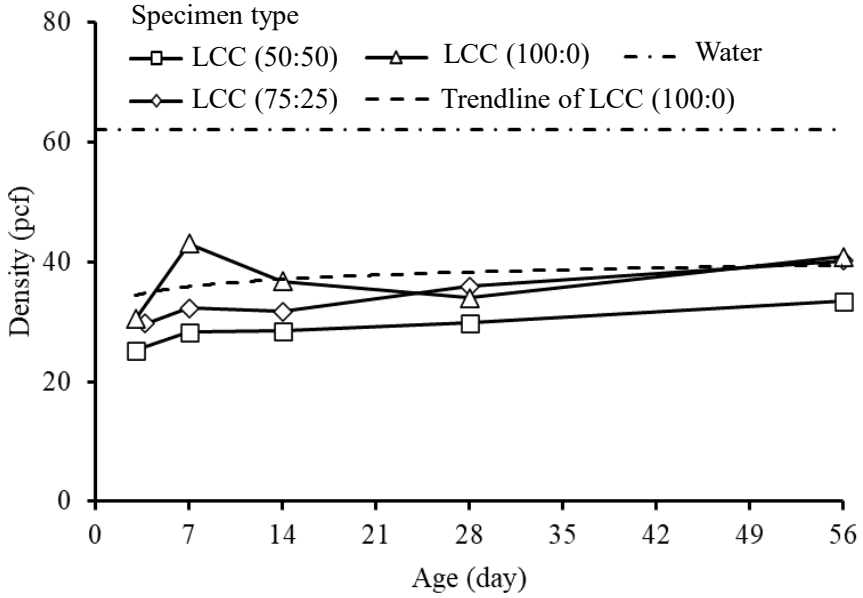

(a) Wet Density

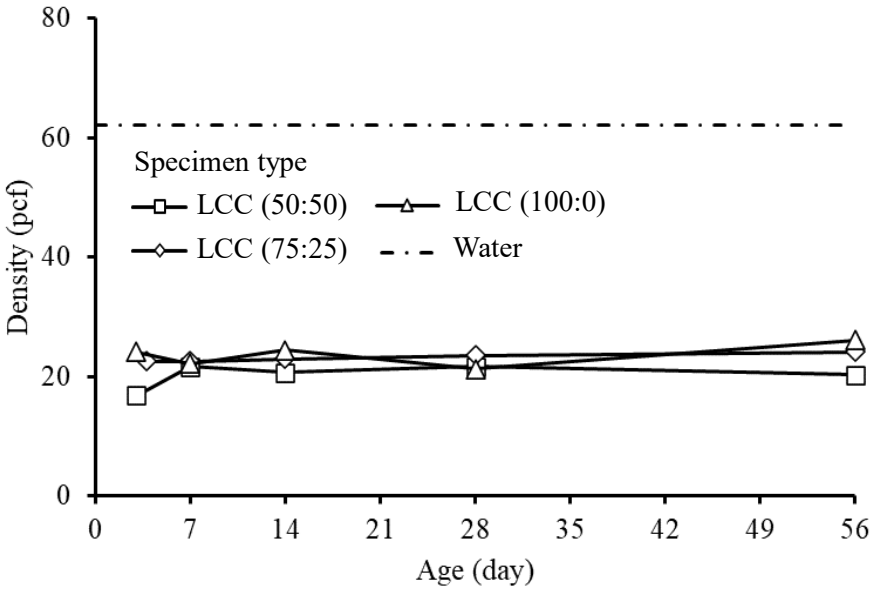

(b) Dry Density

Figure 3.2: Average Density Versus Age of LCC

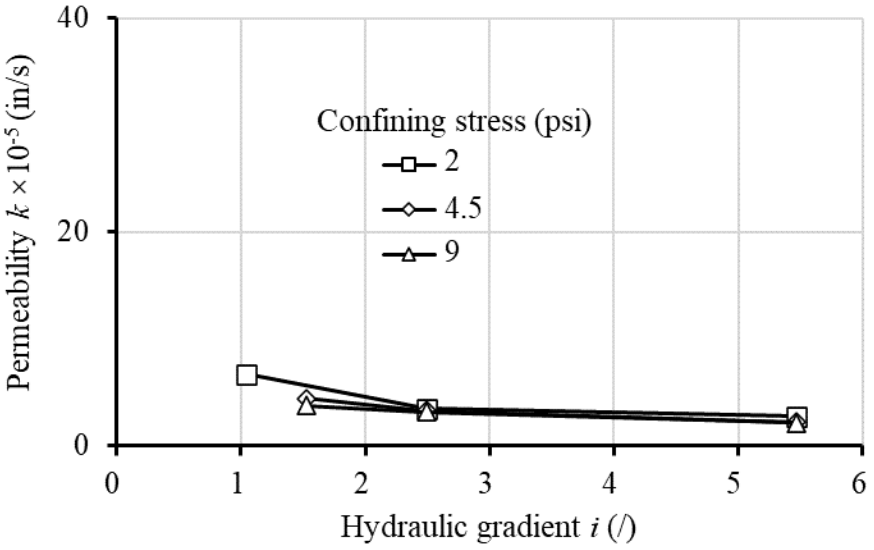

(a) LCC (50:50)

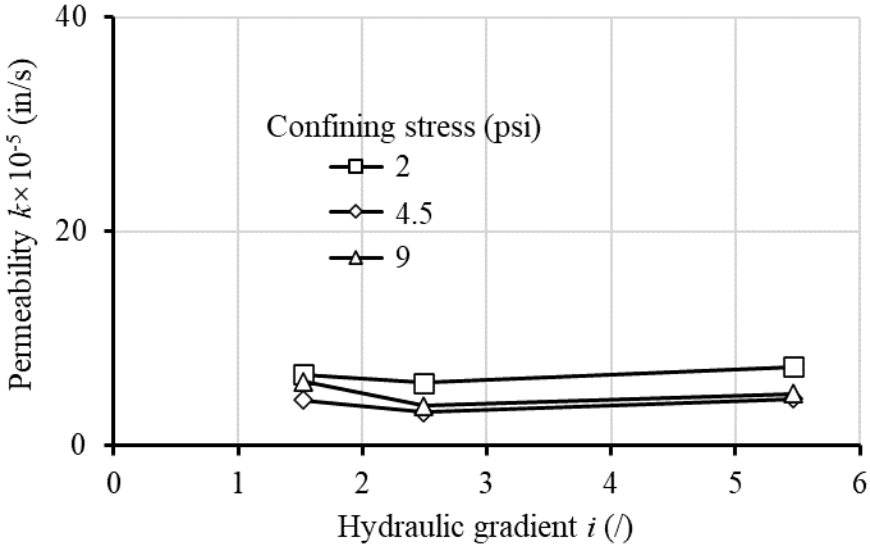

(b) LCC (75:25)-b

Figure 3.3: Permeability Versus the Hydraulic Gradient

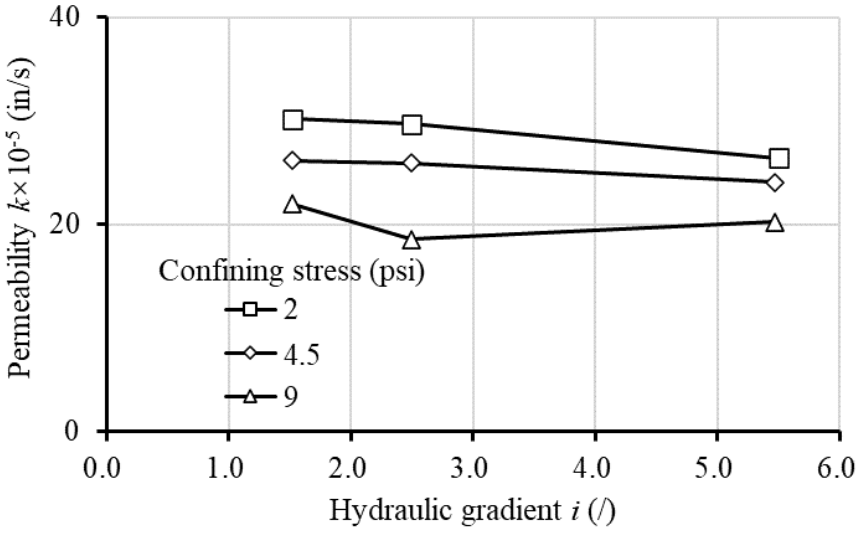

(c) LCC (100:0)

Figure 3.3: Permeability Versus the Hydraulic Gradient (Continued)

Table 3.2: Permeability of LCC at Different Densities

Reference	Backfill type	Wet density (pcf)	Permeability (in./s)
This paper	LCC (50:50)	30	2.1×10^{-5} to 6.7×10^{-5}
	LCC (75:25)-b	34	3.1×10^{-5} to 7.3×10^{-5}
	LCC (100:0)	34	1.9×10^{-4} to 3.0×10^{-4}
Soil Exploration Company (1981)	LCC (-)	-	In the order of 10^{-7}
Tiwari et al. (2017)	LCC (100:0)	19 to 48	6.7×10^{-5} to 4.7×10^{-4}

3.2.3 Unconfined Compressive Strength

Figure 3.4 shows the measured compressive strength of LCC versus the age for all LCC specimens cast in the field. For most mixtures, the compressive strength value for each mix at each age was calculated as an average from typically three specimens; for LCC (75:25)-b, LCC (75:25)-c, and LCC (75:25)-d, only a single specimen was tested at each age due to the limited number of cylinders made of the same mix. Figure 3.4 includes the lines corresponding to the minimum compressive strength for Classes II to VI LCC from ACI 523 (2006). The measured compressive

strengths of LCC specimens are comparable to the minimum compressive strengths suggested by ACI 523 (2006).

Figure 3.5 shows the average unconfined compressive strength values of LCC versus age for further analysis. Since LCC (75:25)-d is considered an outlier, the average density values for LCC (75:25) were calculated based on LCC (75:25)-a, LCC (75:25)-b and LCC (75:25)-c. As expected, the compressive strength increased as the age and the cement to fly ash ratio increased. The LCC (100:0) mix had the most rapid increase in its compressive strength while the LCC (50:50) and LCC (75:25) mixes had a slower increase in their strengths. The drop in the compressive strength of LCC (100:0) at 28 days was caused by the lower density of the mix. Figure 3.5 shows that the average compressive strength ranged from 62 to 167 psi at 28 days. The measured average compressive strengths in this study are consistent with those reported by Narayanan and Ramamurthy (2000) for LCC at a density of 25 pcf. Since the measured compressive strengths of LCC (100:0) had large variations, a trend line based on a two-order logarithmic function was included in Figure 3.5. The compressive strength of LCC (100:0) used for the calculation of elastic modulus later in the paper was determined based on this trendline.

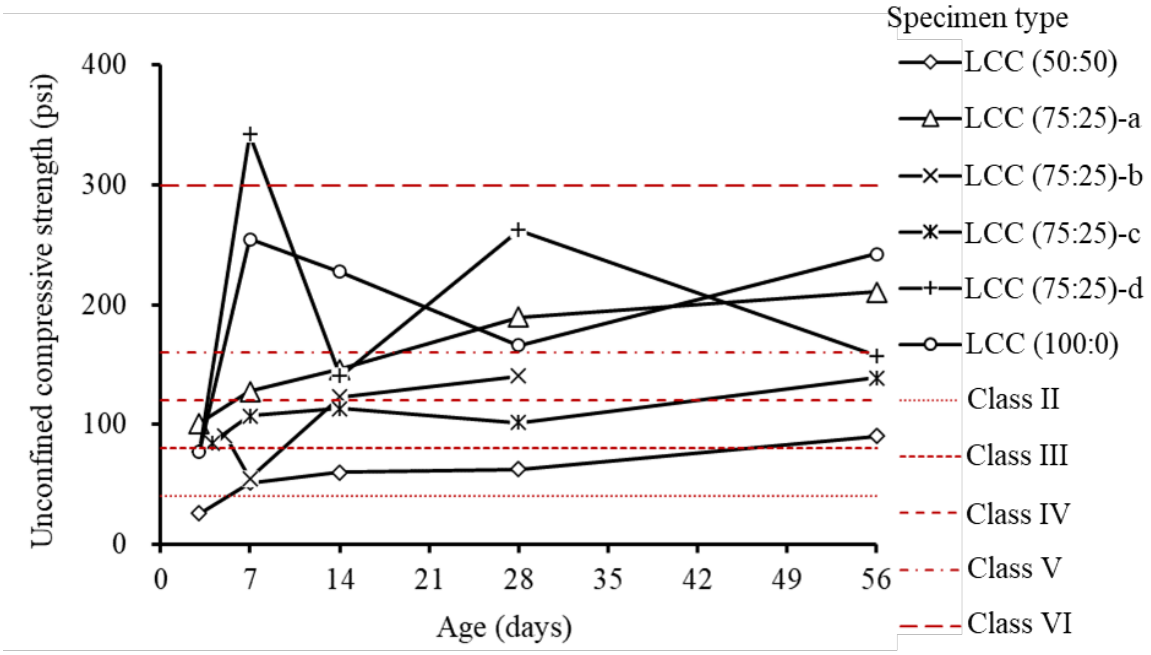

Figure 3.4: Compressive Strength Versus Age

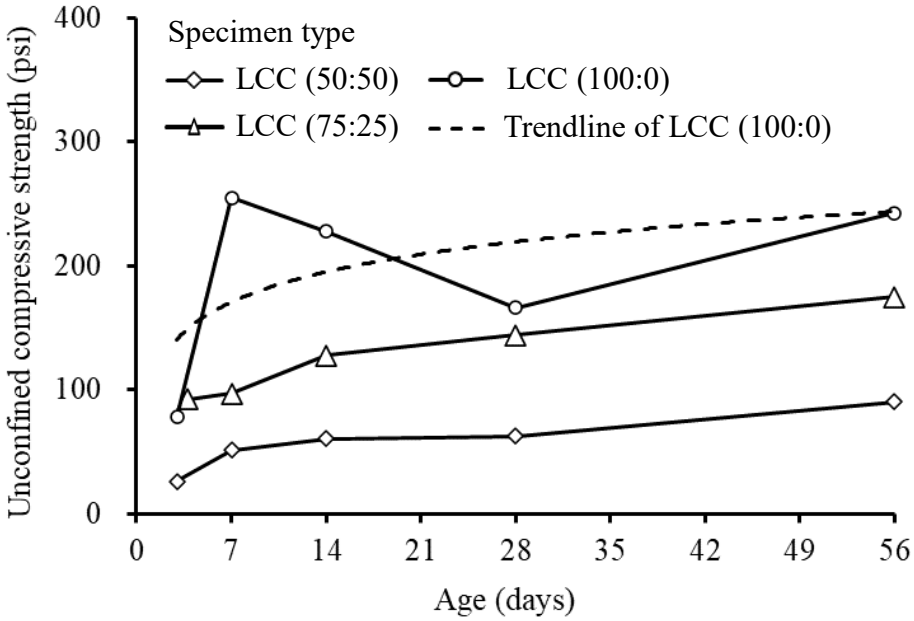

Figure 3.5: Average Compressive Strength Versus Age

3.2.4 Direct Shear Strength

Figures 3.6 and 3.7 show the shear stress versus relative shear displacement for the LCC specimens from the small shear box and large shear box tests, respectively. The relative shear displacement is defined as the ratio of the horizontal shear displacement to the specimen diameter since different specimen sizes were used for these two tests. For the large shear box tests, an equivalent diameter was calculated based on the cross-sectional area of the specimen and used in the calculation of the relative shear displacement. LCC (50:50), LCC (75:50)-b, and LCC (100:0) specimens were used for the direct shear tests. Due to the limited number of prismatic LCC (50:50) specimens, only one large direct shear test on LCC (50:50) was conducted. One extra cylindrical LCC (75:25)-b specimen was used to repeat the small direct shear test at the normal stress of 9 psi. As the relative shear displacement increased, the specimen reached a peak strength and then quickly decreased to a residual strength. Overall, the LCC specimens show brittle behavior. Figures 3.6 and 3.7 show that the shear stress increased as the normal stress increased. The repeat shear test had similar shear behavior as the original test.

The relative shear displacements at peak strengths for the large shear box tests were one-fifth to half those for the small shear box tests as shown in Table 3.3. Table 3.3 also shows that for LCC (50:50), LCC (75:50)-b, and LCC (100:0) in small direct shear box tests, the average peak shear stresses were 26, 38, and 39 psi, while those in the large direct shear box tests were 26, 48, and 51 psi. The ratios of the peak stresses in small direct shear box tests to those in large direct shear box tests were 1.00, 0.79, and 0.76. An average ratio of 0.85 can be considered as a scale factor between the small direct shear box tests and large direct shear box tests on LCC.

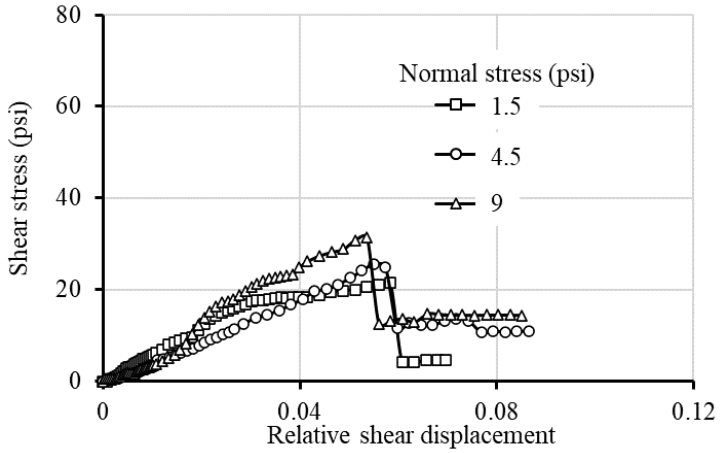

(a) LCC (50:50)

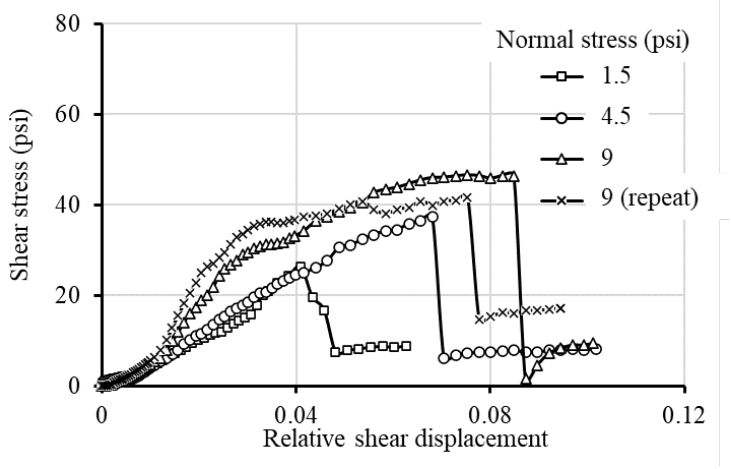

(b) LCC (75:25)-b

Figure 3.6: Shear Stress Versus Relative Shear Displacement for Small Shear Tests

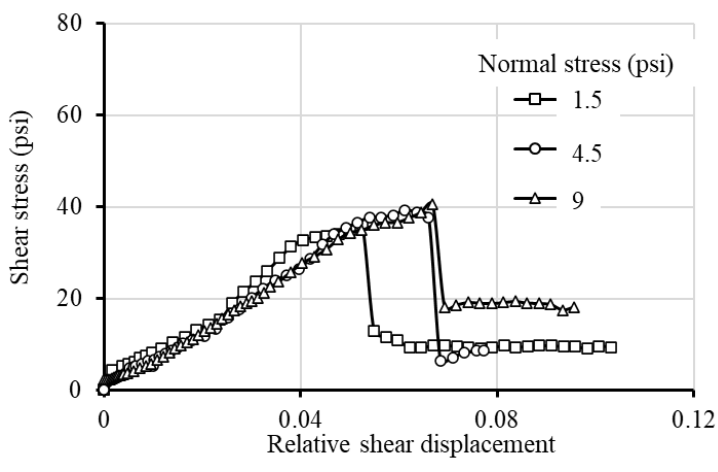

(c) LCC (100:0)

Figure 3.6: Shear Stress Versus Relative Shear Displacement for Small Shear Tests (Continued)

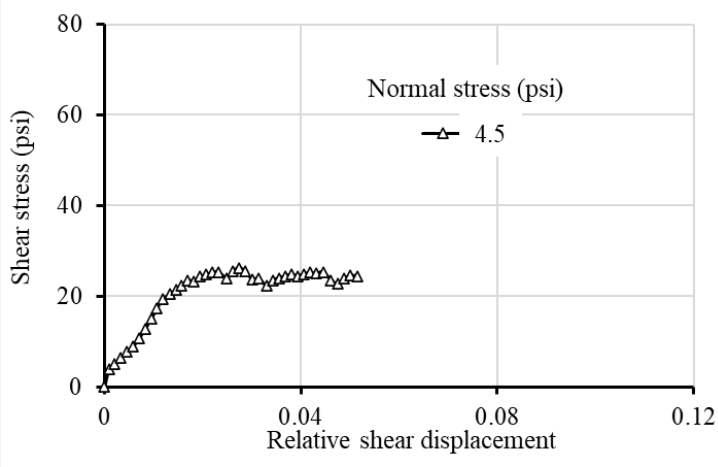

(a) LCC (50:50)

Figure 3.7: Shear Stress Versus Relative Shear Displacement for Large Shear Tests

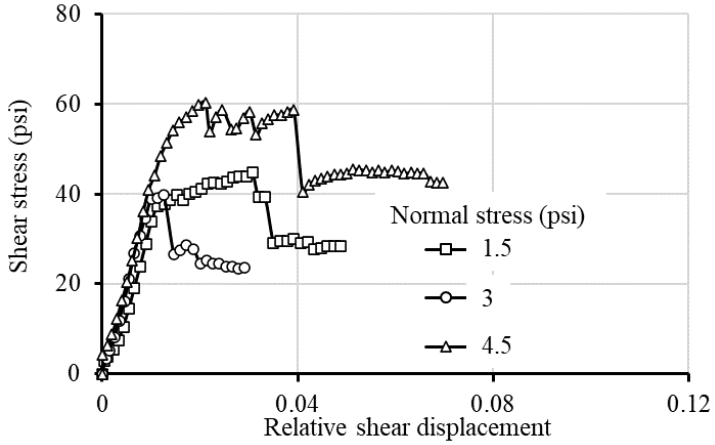

(b) LCC (75:25)-b

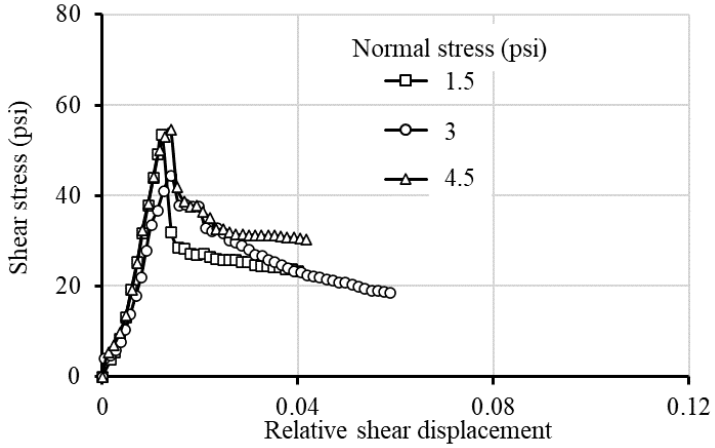

(c) LCC (100:0)

Figure 3.7: Shear Stress Versus Relative Shear Displacement for Large Shear Tests (Continued)

Table 3.3: Peak Shear Stress and the Corresponding Relative Displacement for Direct Shear Tests

Small direct shear test			
Specimen type	Normal stress (psi)	Peak shear stress (psi)	Relative displacement
LCC (50:50)	1.5 4.5 9	21 26 31	0.058 0.055 0.054
Average		26	0.056
LCC (75:25)-b	1.5 4.5 9 9 (Repeat)	26 37 46 42	0.041 0.068 0.085 0.075
Average		38	0.067
LCC (100:0)	1.5 4.5 9	36 39 40	0.052 0.061 0.067
Average		39	0.060
Large direct shear test			
Specimen type	Normal stress (psi)	Peak shear stress (psi)	Relative displacement
LCC (50:50)	4.5	26	0.044
LCC (75:25)-b	1.5 3 4.5	45 40 60	0.031 0.013 0.021
Average		48	0.022
LCC (100:0)	1.5 3 4.5	54 44 55	0.012 0.014 0.014
Average		51	0.013

Figure 3.8 shows the Mohr-Coulomb failure envelopes for the peak and residual strengths of the LCC specimens from small and large shear box tests. For comparison, Figure 3.8 includes a line corresponding to half of the unconfined compressive strengths ($q_u/2$) measured at 28 days for LCC (50:50), LCC (75:25)-b, and LCC (100:0). It is well known that the shear strength of granular material can be calculated using Equation 3.1 as follows:

$$\tau = \sigma \cdot \tan\varphi$$

Equation 3.1

Where: τ is the shear strength, σ is the normal stress, and φ is the internal friction angle of the granular material.

FHWA (Berg et al., 2009) suggested that the friction angle used for design should not exceed 40 degrees. The calculated shear strength of granular material using Equation 3.1 with a friction angle of 40 degrees referred to as the FHWA limit is included in Figure 3.8 for a purpose of comparison.

The shear strengths of the LCC specimens measured in the large direct shear box tests were higher than those in the small direct shear box tests except for LCC (50:50), indicating the specimen scale affected the shear strength of LCC. In general, the LCC specimens behaved like a cohesive material. The peak and residual strengths of LCC (100:0) and LCC (75:25)-b are lower than half of their unconfined compressive strengths ($q_u/2$) measured at 28 days, while the peak strengths of LCC (50:50) from the large direct shear box tests are close to $q_u/2$ measured at the age of 28 days. The shear strength of LCC is approximately four to five times that of the FHWA limit.

Based on the peak strengths, LCC (50:50), LCC (75:25)-b, and LCC (100:0) had cohesion values of 19, 26, and 37 psi, and the friction angles of 54, 63, and 19 degrees, respectively from the small shear box tests while LCC (75:25)-b and LCC (100:0) had the cohesion values of 33 and 50 psi and the friction angles of 79 and 23 degrees from the large shear box tests. The test results show that the LCC specimens with the cement to fly ash ratio of 75:25 had the largest friction angle while the cohesion value of the LCC specimen increased as the cement to fly ash ratio increased.

The empirical formulae developed by Tiwari et al. (2017) and presented in Equations 2.1 and 2.2 predicted that LCC (50:50), LCC (75:25)-b, and LCC (100:0) should have friction angles of 20, 21, and 22 degrees and cohesion values of 92, 116, and 162 psi. In these calculations, the measured wet densities for LCC (50:50), LCC (75:25)-b, and LCC (100:0) at the age of 28 days were used. The calculated friction angles for LCC (50:50) and LCC (100:0) are close to the measured while the calculated friction angle for LCC (75:25)-b is significantly smaller than the measured.

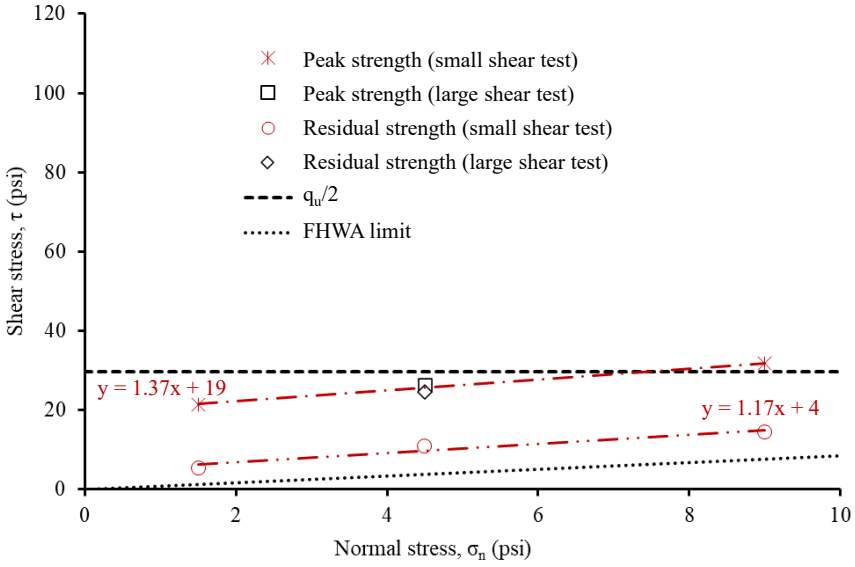

(a) LCC (50:50)

Figure 3.8: Mohr-Coulomb Failure Envelopes

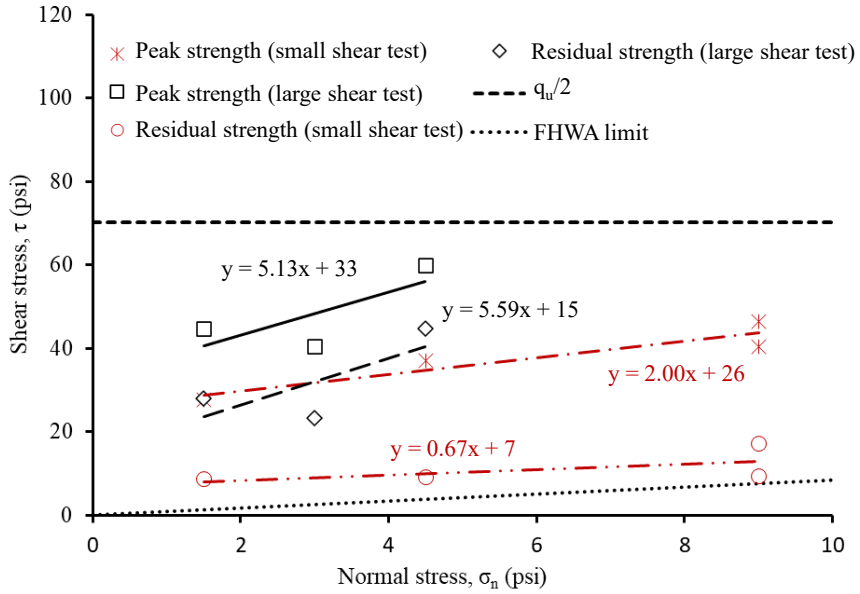

(b) LCC (75:25)-b

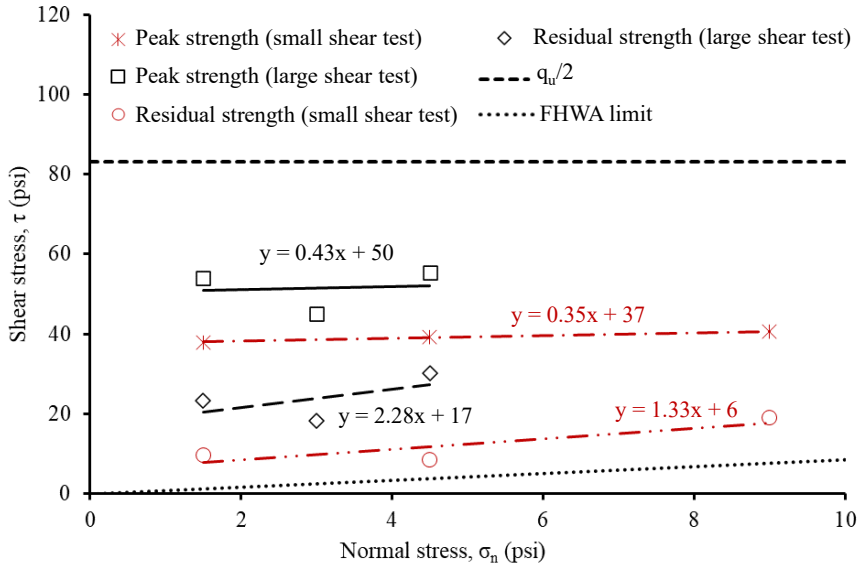

(c) LCC (100:0)

Figure 3.8: Mohr-Coulomb Failure Envelopes (Continued)

Considering the LCC specimens behaved like a cohesive material, the average shear strengths, friction angles, and cohesions for all three types of LCC were calculated and are presented in Table 3.4. For comparison, Table 3.4 also includes half, one-third, and one-quarter of the compressive strengths (i.e., $q_u/2$, $q_u/3$, and $q_u/4$) of LCC measured at 28 days. The peak cohesion increased as the cement to fly ash ratio increased. The average peak strengths of LCC (75:25)-b and LCC (100:0) were close to $q_u/3$ or $q_u/4$. Table 3.4 shows that the residual to peak strength ratios from the small shear box tests were approximately half those from the large shear box tests.

3.2.5 Elastic Modulus and Poisson's Ratio

LCC (75:25)-a and LCC (100:0) were used for elastic modulus and Poisson's ratio tests. The measured elastic moduli LCC (75:25)-a and LCC (100:0) were 286 and 189 ksi, respectively. These measured elastic moduli are close to the estimated elastic moduli of 180 to 267 ksi at the dry density of 31 pcf based on Narayanan and Ramamurthy (2000). Poisson's ratios for LCC (75:25)-a and LCC (100:0) were determined as 0.35 and 0.34, respectively, based on the measured strains. These values are larger than those measured Poisson's ratios in Tiwari et al. (2017) ranging from 0.2 to 0.3.

Table 3.4: Summary on Direct Shear Test Results

Small direct shear box test			
Specimen type	LCC (50:50)	LCC (75:25)-b	LCC (100:0)
Average peak strength (psi)	26	38	39
Average residual strength (psi)	10	11	12
Residual to peak strength ratio	0.39	0.29	0.32
Peak friction angle (degree)	54	63	19
Residual friction angle (degree)	50	34	53
Peak cohesion (psi)	19	26	37
Residual cohesion (psi)	4	7	6
$q_u/2$ (psi)	21	47	55
$q_u/3$ (psi)	16	35	42
$q_u/4$ (psi)	3	7	8
Large direct shear box test			
Specimen type	LCC (50:50)	LCC (75:25)-b	LCC (100:0)
Average peak strength (psi)	26	48	51
Average residual strength (psi)	25	32	24
Residual to peak strength ratio	0.93	0.66	0.47
Peak friction angle (degree)	-	79	23
Residual friction angle (degree)	-	80	66
Peak cohesion (psi)	-	33	50
Residual cohesion (psi)	-	15	17
$q_u/2$ (psi)	21	47	55
$q_u/3$ (psi)	16	35	42
$q_u/4$ (psi)	3	7	8

Table 3.5 shows the comparison of the measured elastic moduli in this study with the calculated values using the correlations obtained by Tada (1986) and Jones and McCarthy (2005b) based on the wet density and the compressive strength measured at 28 days in this study. Previous density and unconfined compression tests show that the measured wet densities of LCC (75:25)-a and LCC (100:0) were 40 and 39 pcf, respectively, and the unconfined compressive strengths of LCC (75:25)-a and LCC (100:0) were 190 and 219 psi, respectively at the age of 28 days. The measured wet density and unconfined compressive strength for LCC (100:0) were determined based on its trendline. Table 3.5 shows that for LCC (100:0), the calculated elastic moduli using the Jones and McCarthy (2005b) correlation better matched the measured values than that using the Tada (1986) correlation. For the LCC (75:25)-a specimen, the calculated elastic moduli using the Jones and McCarthy (2005b) correlation was lower than the measured, while the calculated elastic moduli using the Tada (1986) correlation was higher than the measured.

Table 3.5: Predicted and Measured Elastic Moduli of LCC

Reference	Elastic modulus (ksi)	
	LCC (75:25)-a	LCC (100:0)
This paper	286	189
Tada (1986)	364	348
Jones and McCarthy (2005b)	173	186

The relationship between the shear modulus, the elastic modulus, and Poisson's ratio is given in Equation 3.2:

$$G = \frac{E}{2(1+v)}$$

Equation 3.2

Where: E is the elastic modulus, v is Poisson's ratio, and G is the shear modulus.

The calculated shear moduli of LCC (75:25)-a and LCC (100:0) are 106 and 71 ksi based on the elastic moduli and Poisson's ratios measured in this study.

3.2.6 One-Dimensional Consolidation

Figure 3.9 shows the variations of the strain ε versus the normal stress σ of the LCC specimen. The wet density values for LCC (50:50), LCC (75:25)-b, and LCC (100:0) used in the consolidation tests were 30, 34, and 34 pcf. Based on the curves in Figure 3.9, the yielding stresses for LCC (50:50), LCC (75:25)-b, and LCC (100:0) were 28, 33, and 31 psi, which are approximately correlated to their density values. The yielding stresses of the LCC specimens were lower than the corresponding unconfined compressive strengths as described in the previous section. The specimens used for the consolidation tests were saturated and the saturation might have reduced the strength of LCC. For the corresponding LCC in terms of the wet density in Tiwari et al. (2017), its yielding stress was 29 psi, which is close to the measured values in this study.

From Figure 3.9, the recompression indices $C_{r\varepsilon}$ for LCC (50:50), LCC (75:25)-b, and LCC (100:0) were determined as 7.2×10^{-3}, 6.2×10^{-3}, and 6.5×10^{-3}, respectively, and their compression indices $C_{c\varepsilon}$ were 8.9×10^{-2}, 4.1×10^{-2}, and 1.1×10^{-1}, respectively. The average compression index of LCC (50:50), LCC (75:25)-b, and LCC (100:0) was approximately 12 times the recompression index.

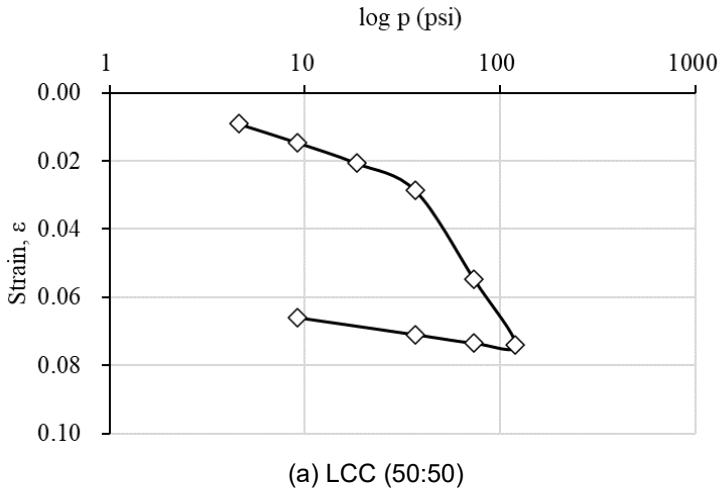

Figure 3.9: Strain Versus Normal Stress Curves in Consolidation Test

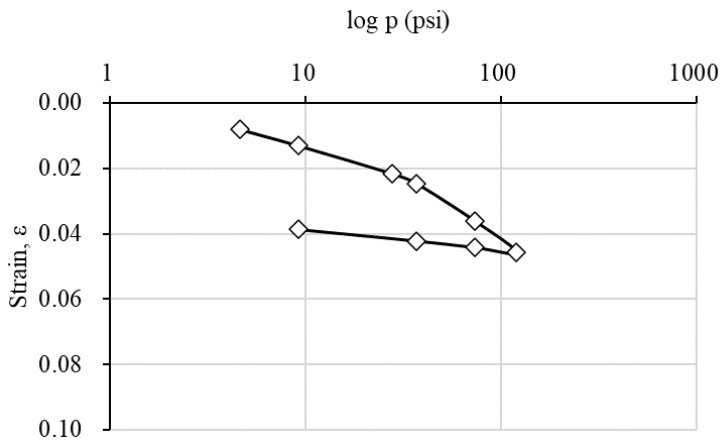

(b) LCC (75:25)-b

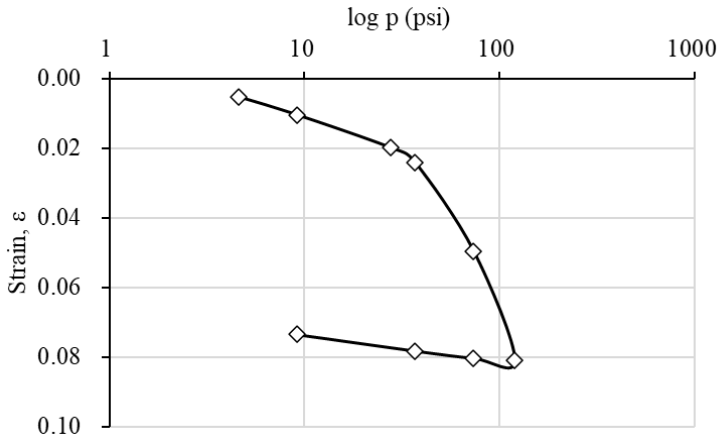

(c) LCC (100:0)

Figure 3.9: Strain Versus Normal Stress Curves in Consolidation Test (Continued)

Chapter 4: Laboratory Pullout Tests

This chapter presents a series of pullout tests performed in the laboratory using a large pullout box to investigate the pullout resistance of geogrid (extensible reinforcement) and steel strip (inextensible reinforcement) embedded in LCC. This laboratory study evaluated the effects of age, normal stress, fly ash, presence of a cold joint, and re-pullout on the pullout resistance and calculated the pullout resistance factors F^* for geogrid and steel strip embedded in LCC.

4.1 Test Set-up and Program

4.1.1 Materials

4.1.1.1 Geogrid and Steel Reinforcement

Figure 4.1(a) shows the plan view of the uniaxial geogrid reinforcement in the LCC specimen. The geogrid used in the study was manufactured by a punching-drawn process of high-density polyethylene (HDPE) material. This geogrid had an effective length L_e (the embedded length in the LCC specimen) of 55 inches, a width of 16.5 inches, and a thickness of 0.1 inches. The aperture size of this geogrid was 0.6 inches wide and 17.7 inches long. This geogrid had a tensile strength at 5% strain of 3.6 kips/ft and ultimate tensile strength of 7.8 kips/ft. Figure 4.1(b) shows the plan view of the ribbed steel strip reinforcement placed in the LCC specimen. This steel strip had a yield strength of 65 ksi, an effective length L_e of 55 inches (equal to that of the geogrid), a width of 2 inches, and a thickness of 0.2 inches. The ribs on both the top and bottom faces of the steel strip were 0.1 inches high.

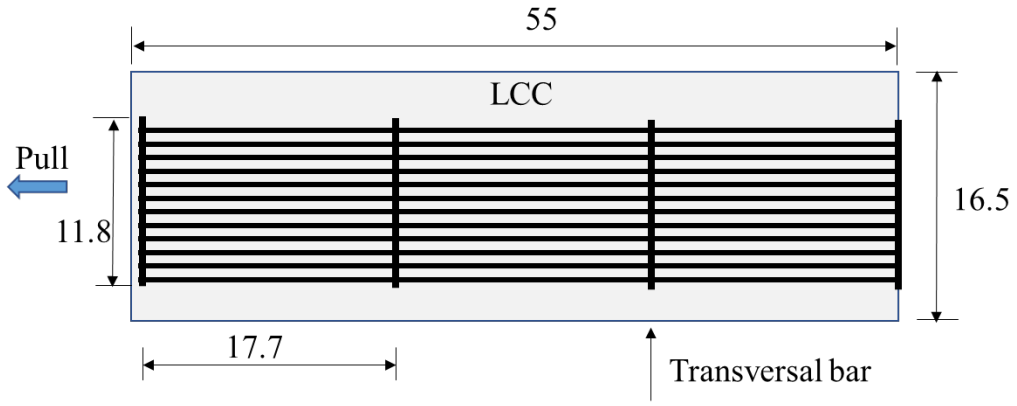

(a) Geogrid-Reinforced LCC

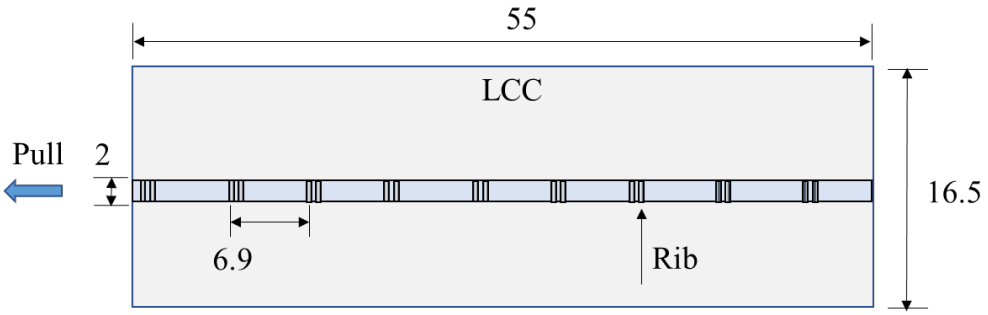

(b) Steel Strip-Reinforced LCC

Figure 4.1: Plan View of Extensible (Geogrid) Reinforcement and Inextensible (Steel Strip) Reinforcement (Unit: in.)

4.1.1.2 LCC materials

This research includes two types of LCC materials with cement to fly ash ratios of 75:25 and 100:0, which are designated as LCC (75:25) and LCC (100:0). The target water to cement ratio of the LCC was 0.55. LCC specimens with each mix were cast in both cylindrical and prismatic molds on a project site to better represent field conditions. Cylindrical specimens of approximately 3 inches in diameter and 6 inches in height were used for the density and unconfined compression tests, while prismatic specimens were used for pullout tests to be discussed later. Table 4.1 shows the test schedule for density and unconfined compression tests.

Table 4.1: Wet Density and Unconfined Compression Tests

Specimen type	Water to cement ratio	Cement to fly ash ratio	Cast date	Test age (days)
LCC (75:25)	0.55	75:25	Sept. 28, 2020	3, 7, 14, 28 and 56
LCC (100:0)	0.55	100:0	Oct. 01, 2020	3, 7, 14, 28 and 56

Figure 4.2 shows the wet density versus age for the LCC specimens. The wet density value for each mix at each age was calculated as an average from three specimens. For LCC (75:25) and LCC (100:0), the measured wet densities became stable after 7 days. The measured wet densities ranged from 34 to 40 pcf at the age of 28 days. Based on Ozlutas (2015), the LCC materials used in this study are considered as ultra-low density cellular concrete. Based on Engineered Fill (2001), they are classified as Classes III and IV LCC. Figure 4.2 also shows the density of water, which is higher than those of both LCC mixes.

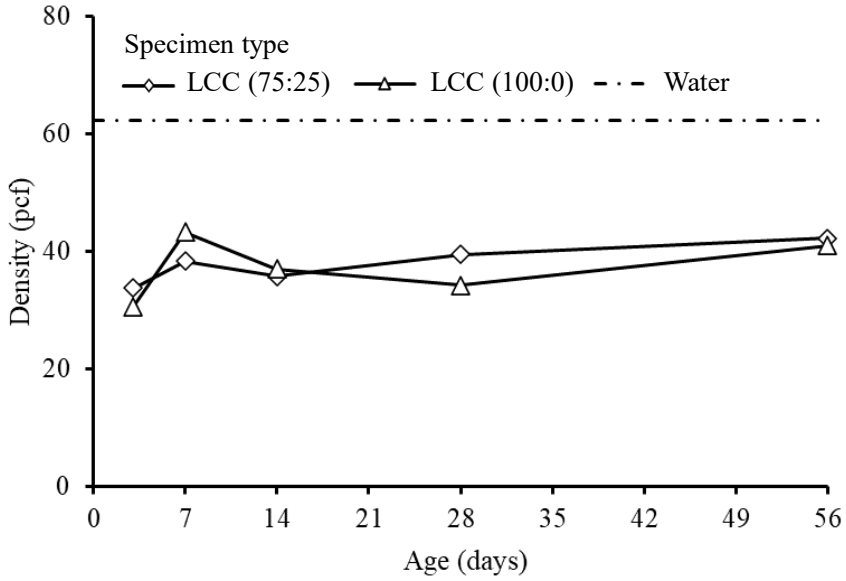

Figure 4.2: Variations of Wet Density Versus Age for LCC

Figure 4.3 shows the variations of the unconfined compressive strength versus age for these two LCC materials. The compressive strength for each mix for a given age was calculated as an

average from three specimens. In general, the compressive strength increased with age. The measured compressive strength ranged from 160 to 189 psi at the age of 28 days. Considering the variability of the LCC (100:0) test results, a trend line is provided for this mix in Figure 4.3, showing it had higher compressive strengths than the LCC (75:25) mix. The higher strength at the age of 7 days and the lower strength at the age of 28 days for the LCC (100:0) specimens correspond to their densities at the same ages as shown in Figure 4.2.

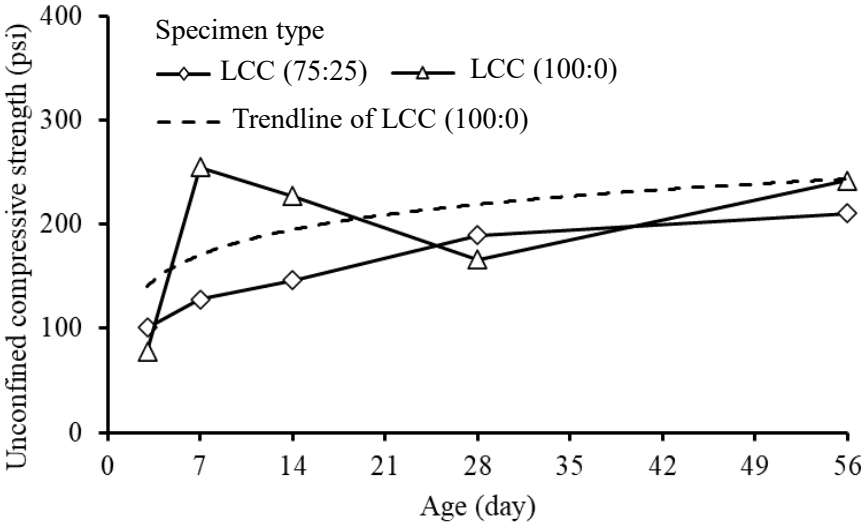

Figure 4.3: Variations of Unconfined Compressive Strength Versus Age for LCC Specimens

All pullout specimens were cast into pre-fabricated wood molds on the field project site as shown in Figure 4.4, cured overnight, and then transported back to the laboratory at the University of Kansas for continued curing within a temperature-controlled and moisture-controlled environment. Each LCC specimen for a pullout test was 55 inches long, 16.5 inches wide, and 11 inches high so that it could be fit into the pullout box.

Figure 4.4: Pullout Specimens Cast on a Project Site

4.1.2 Pullout Box

The large pullout box used in this study was designed and fabricated by the research group at the University of Kansas to study the pullout resistance of extensible (geogrids) and inextensible (steel strips) reinforcement (Rahmaninezhad, Han, Kakrasul, & Weldu, 2019). The pullout box is composed of a metal box, a clamp, LVDT, a load cell, a hydraulic jack, and a data acquisition system. The metal box is made of steel with inner dimensions of 59 inches long, 18 inches wide, and 24 inches high, meeting the requirements of ASTM D6706 (2013). A hydraulic jack with an oil pump applied a horizontal pullout force to the reinforcement through the clamp; the pullout force was measured by a load cell. Displacement transducers (LVDT) measured the displacements of the reinforcement in the front (loaded end) and rear (unloaded end). The pullout displacement rate was controlled by the hydraulic jack. Figure 4.5 shows the cross-sectional view of the pullout test setup. An airbag was used to apply normal stress on the top surface of the LCC specimen. A layer of nonwoven geotextile was placed between the airbag and the LCC specimen to ensure full contact and protect the airbag. Wood panels were placed at the bottom and rear of the pullout box to adjust the inner dimensions so that the reinforcement was aligned with the clamp, the load cell, and the hydraulic jack.

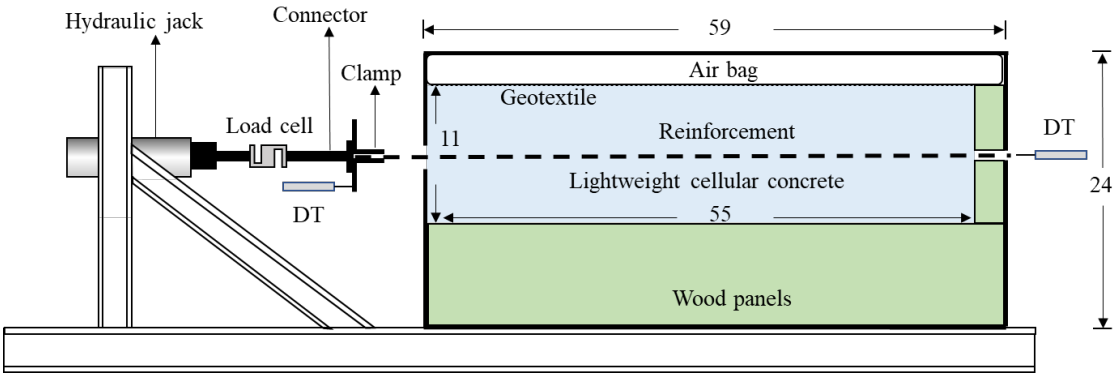

Figure 4.5: Cross-Sectional View of Pullout Test Setup (unit: in.)

4.1.3 Test Procedure

Pullout tests were conducted at 7, 14, and 28 days; re-pullout tests were conducted at 35 days on the specimens previously tested at 7 or 14 days. Each LCC specimen (with embedded reinforcement) was removed from the wood mold and put into the pullout test box according to the test schedule as shown in Table 4.2. The free end of the reinforcement was fixed into a clamp. For geogrid reinforcement, the clamp had multiple holes; several steel screws went through these holes and the apertures of the geogrid to secure the grid. For the steel strip, a single hole was drilled in the front end of the strip; a single steel screw was used to secure the strip to the clamp. The clamp was attached to the load cell, which in turn was connected to the hydraulic jack assembly. An airbag was placed on the top of the LCC specimen to apply normal stress. To simulate the pullout resistance of reinforcement in LCC backfill at different elevations in a wall, three normal stresses of 1.5, 4.5, and 9 psi were selected. Previous research (Liu, Zhu, Wang, & Shi, 2019) found that a pullout displacement rate of 0.002 in./s approximated static loading. Based on the minimum pullout displacement rate the hydraulic jack could apply, the pullout displacement rate was selected as 0.003 in./s to simulate the static pullout loading condition as closely as possible. The pullout test was terminated when the front displacement of the reinforcement reached a sufficient magnitude or when the reinforcement broke at the clamp.

4.1.4 Testing Program

A total of 44 pullout tests are reported in this paper, as listed in Table 4.2. These pullout tests evaluated three normal stresses, two LCC mixes, two reinforcement types, three ages, the cold joint effect, and the re-pullout effect. Tests T1 to T36 were normal pullout tests. Tests C1, C2, and C3 were pullout tests with a cold joint between the steel strip and LCC. Re-pullout tests R1, R2, R3, R4, and R5 were conducted on the pre-tested specimens (T4, T5, T19, T20, and T21) at an age of 35 days.

Table 4.2: Pullout Tests

Test ID	Normal stress (psi)	Reinforcement	Ages (days)	Cement to fly ash ratio
T1, T2, T3	1.5, 4.5, 9	Geogrid	7	75:25
T4, T5, T6		Geogrid		100:0
T7, T8, T9		Steel strip		75:25
T10, T11, T12		Steel strip		100:0
T13, T14, T15	1.5, 4.5, 9	Geogrid	14	75:25
T16, T17, T18		Geogrid		100:0
T19, T20, T21		Steel strip		75:25
T22, T23, T24		Steel strip		100:0
T25, T26, T27	1.5, 4.5, 9	Geogrid	28	75:25
T28, T29, T30		Geogrid		100:0
T31, T32, T33		Steel strip		75:25
T34, T35, T36		Steel strip		100:0
C1, C2, C3	4.5	Steel strip	7, 14, 28	75:25
R1, R2	1.5, 4.5	Geogrid	35	75:25
R3, R4, R5	1.5, 4.5, 9	Steel strip		

4.2 Test Results and Discussion

4.2.1 Pullout Resistance

Figures 4.6 and 4.7 show the pullout force versus front displacement for geogrids and steel strips, respectively, in the pullout tests conducted at 7 days. For the geogrid-reinforced LCC specimens, Figure 4.6 shows that the peak pullout forces of the geogrids in LCC (75:25) and LCC

(100:0) ranged from 2.4 to 3.8 and 1.8 to 3.4 kips/ft, respectively, under the normal stresses of 1.5, 4.5, and 9 psi. For each type of LCC, the peak pullout force substantially increased when the normal stress increased. The dependency of the peak pullout force on the normal stress for the geogrid reinforcement is because the geogrid width was close to the specimen width and almost all the applied load from the air bag was applied on the geogrid. For the geogrid-reinforced LCC specimens with the normal stress of 1.5 psi in Figure 4.6a, the geogrid broke during the pullout tests. This breakage happened when screws in the clamp cut through the transverse bar of the geogrid because fewer screws were used in earlier tests. To avoid this problem, more screws were added on the clamp in later pullout tests.

For the steel strip-reinforced LCC specimens, there was no clear relationship between the pullout resistance and the normal stress. This phenomenon might be due to the fact that the steel strip was much narrower than the LCC specimen and when the bond between the steel strip and concrete broke, arching was formed around the steel strip so that the applied load was transferred to the surrounding concrete. Arching is typically defined as load transfer between a yielding portion and adjoining stationary portions (also called supports) under or within a fill, and involves a redistribution of stresses in the fill. However, the pullout resistance depended on the type of LCC. Overall, LCC (100:0) tended to result in a higher pullout resistance than LCC (75:25), likely due to the higher compressive strength of LCC (100:0). The peak pullout forces per unit width for the steel reinforcement were higher than those for the geogrid reinforcement per unit width. The reason is that steel strip reinforcement had more ribs and larger contact areas per unit width than the geogrid reinforcement due to its apertures.

The pullout response for the steel strip in LCC (100:0) (Figure 4.7b) shows softening behavior after reaching the peak. Ramezani et al. (2013) indicated that the interface resistance between steel strip and concrete consisted of three components: chemical bonding, friction resistance, and bearing resistance. Prior to an initial slip, the resistance is due to chemical bonding (similar to adhesion), which is not dependent on a normal stress. After the chemical bond breaks, the interface resistance is primarily provided by the bearing resistance of the ribs on the steel strip and the friction between the LCC and the steel strip surface. The friction depended on the normal stress, however, due to arching effects after the bond between the steel reinforcement and LCC

broke, the normal stress on the steel reinforcement might decrease. This may have contributed to the softening pullout behavior of the steel reinforcement in the LCC.

Figures 4.8 and 4.9 show the pullout force versus front displacement for geogrids and steel strips, respectively, in the pullout tests conducted at 14 days. The responses of the pullout force versus the front displacement at 14 days are similar to those at 7 days, i.e., the normal stress having a significant effect on the pullout resistance for the geogrid reinforcement but a minor effect on that for the steel reinforcement. For the geogrid-reinforced LCC under a normal stress of 4.5 or 9 psi, the pullout force increased up to the peak value and then remained close to the peak value with the increase of the displacement, exhibiting hardening behavior. For the geogrid-reinforced LCC under a normal stress of 1.5 psi, softening pullout behavior occurred after the peak. The softening behavior might result from the dilation of the specimen under the low normal stress after the bond between the geogrid and the LCC broke. For the steel strip-reinforced LCC, the pullout force first increased with the displacement up to the peak values and then decreased to a residual value, exhibiting softening behavior regardless of normal stress.

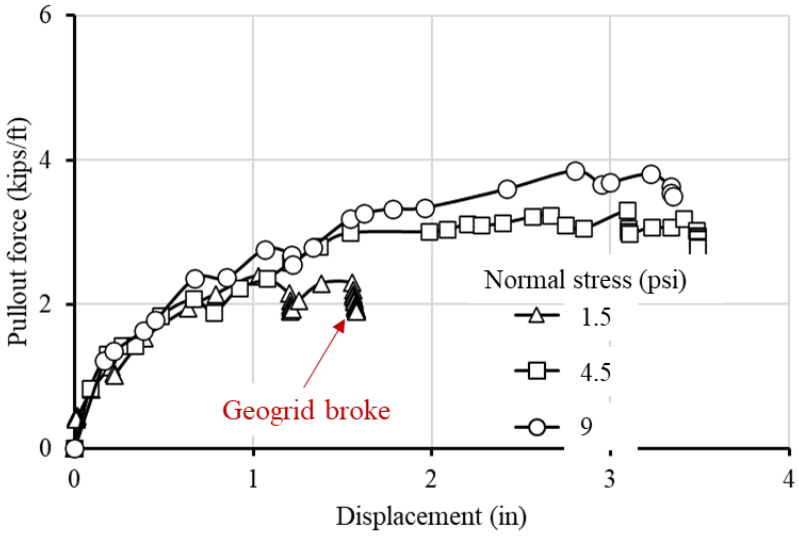

(a) Geogrid-Reinforced LCC (75:25)

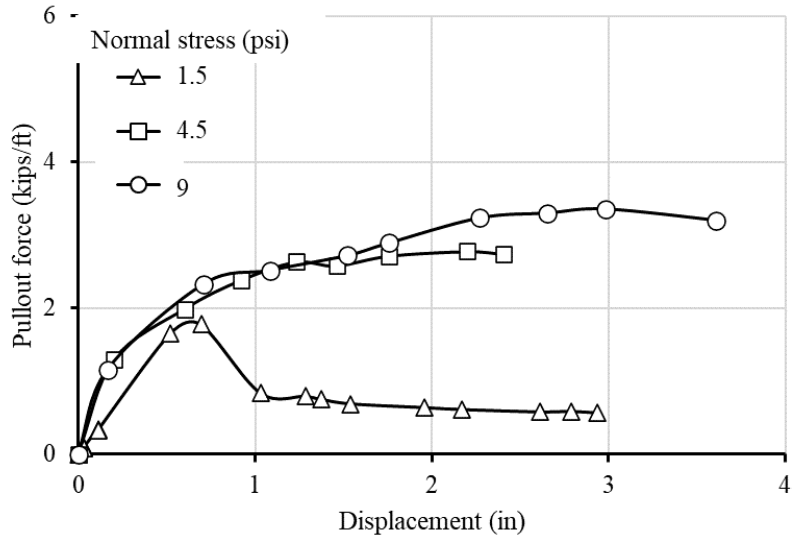

(b) Geogrid-Reinforced LCC (100:0)

Figure 4.6: Pullout Force Versus Front Displacement for Geogrid at 7 Days

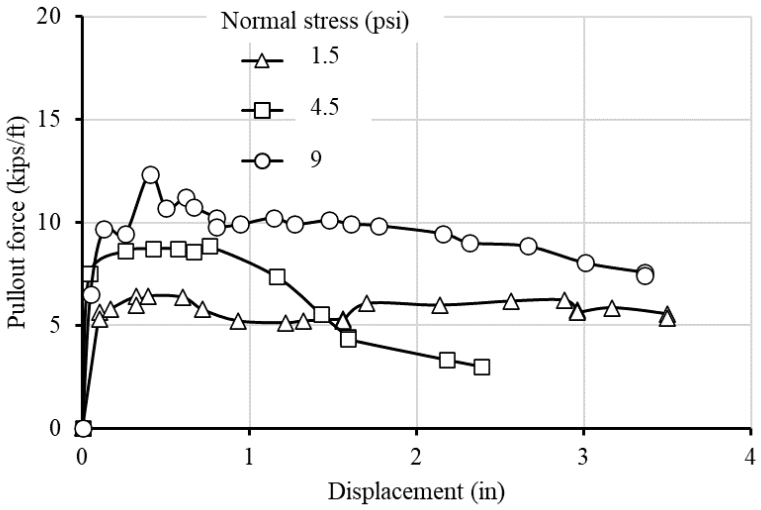

(a) Steel Strip-Reinforced LCC (75:25)

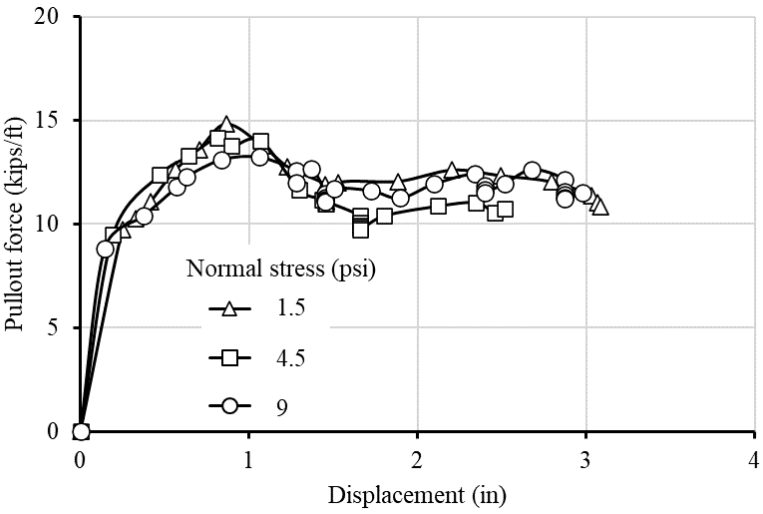

(b) Steel Strip-Reinforced LCC (100:0)

Figure 4.7: Pullout Force Versus Front Displacement for Strip Steel at 7 Days

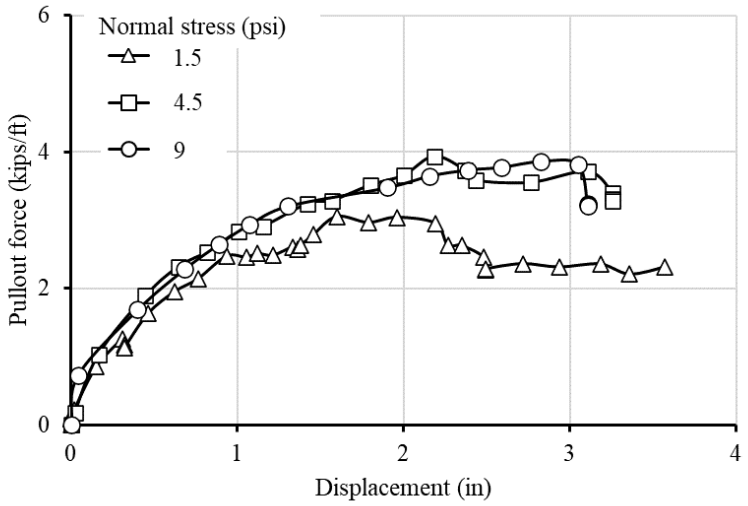

(a) Geogrid-Reinforced LCC (75:25)

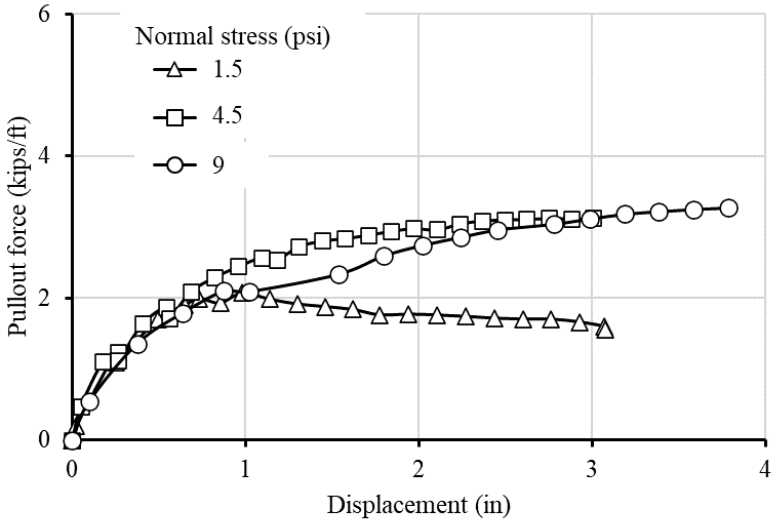

(b) Geogrid-Reinforced LCC (100:0)

Figure 4.8: Pullout Force Versus Front Displacement for Geogrid at 14 Days

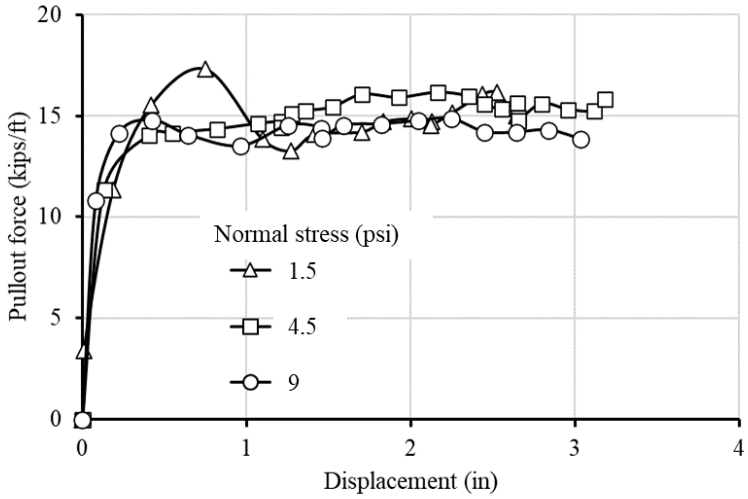

(a) Steel Strip-Reinforced LCC (75:25)

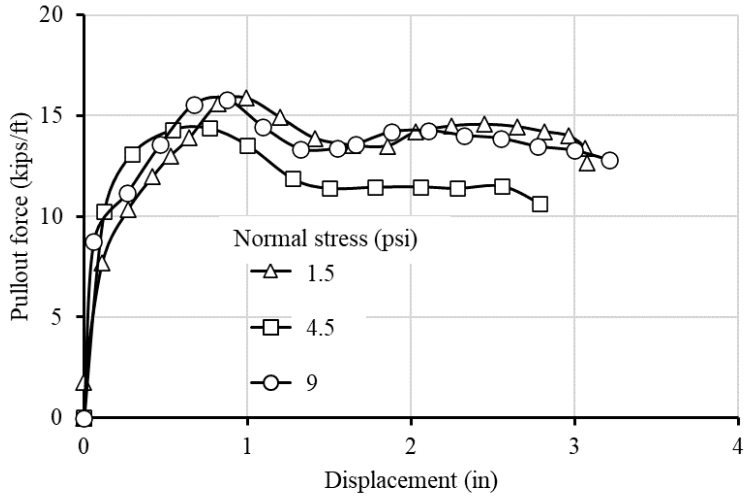

(b) Steel strip-reinforced LCC (100:0)

Figure 4.9: Pullout Force Versus Front Displacement for Steel Strip at 14 Days

Figures 4.10 and 4.11 show the pullout force versus front displacement for geogrids and steel strips, respectively, in the pullout tests conducted at 28 days. The responses of the pullout force versus the displacement were similar to those from the tests conducted at 7 days and 14 days. As described in the previous subsection, the geogrid-reinforced LCC at low normal stress showed softening pullout behavior, while the geogrid-reinforced LCC at higher normal stresses showed hardening pullout behavior. The steel strip-reinforced LCC showed softening pullout behavior at

all normal stresses. For the geogrid-reinforced LCC specimen at a normal stress of 9 psi, Figure 4.10a shows that the geogrid broke during the pullout test. This breakage was induced by the fact that the geogrid was not evenly clamped, and some longitudinal bars broke due to the stress concentration.

FHWA (Berg et al., 2009) recommended the use of a maximum allowable front displacement of a reinforcement in granular and cohesive soils with low plasticity to estimate its design pullout resistance, i.e., 1 to 2 inches for extensile reinforcement (e.g., geogrids) or 0.5 inches for inextensible reinforcement (e.g., ribbed steel strips). The pullout test results in this study show that for the geogrid-reinforced LCC conducted at 28 days, the displacement required for the pullout force to reach the peak value increased with the normal stress. For the steel strip-reinforced LCC, the displacements required to reach the peak pullout forces approximately ranged from 0.4 to 1 inch, which are larger than the allowable values suggested by FHWA (Berg et al., 2009). Rahmaninezhad et al. (2019) conducted pullout tests on a steel strip embedded in sand under a normal stress of 10 psi and obtained a displacement of 0.6 inches at the peak value, suggesting that the displacement at the peak force in LCC is comparable to that in traditional backfill material.

Figures 4.12 and 4.13 show the peak pullout force versus age for geogrids and steel strips in LCC specimens. For the LCC without fly ash (i.e., LCC (100:0)), the pullout resistance slightly increased from 7, 14, to 28 days. Replacing some of cement with fly ash resulted in delayed strength gain; specimens with LCC (75:25) showed increases in the pullout strength from 7 to 14 days before leveling off.

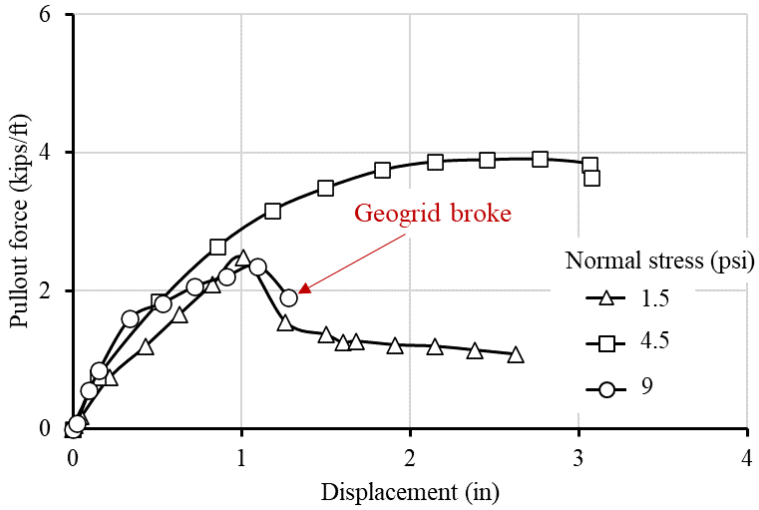

(a) Geogrid-Reinforced LCC (75:25)

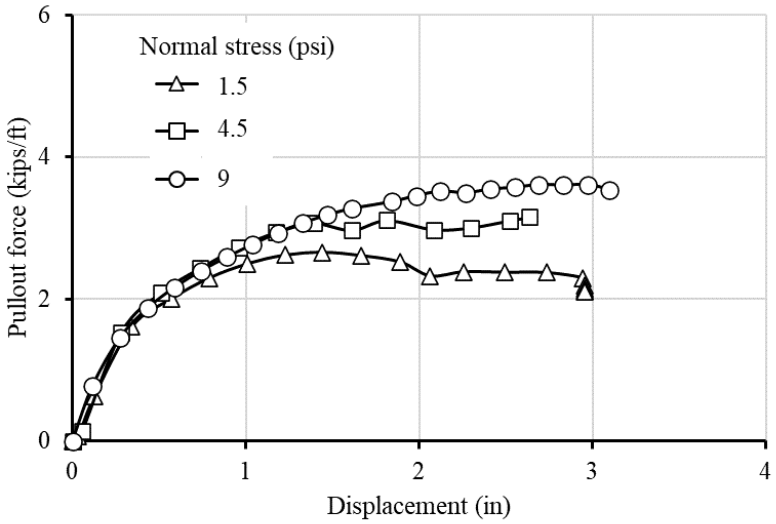

(b) Geogrid-Reinforced LCC (100:0)

Figure 4.10: Pullout Force Versus Front Displacement for Geogrid at 28 Days

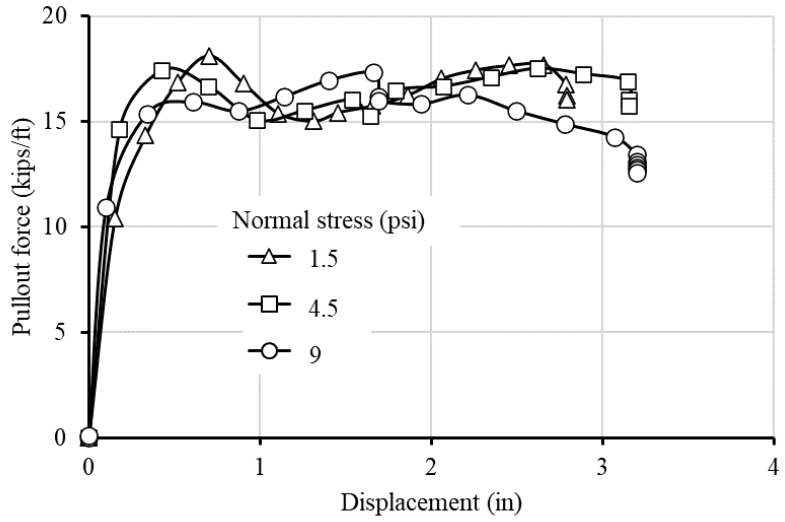

(a) Steel Strip-Reinforced LCC (75:25)

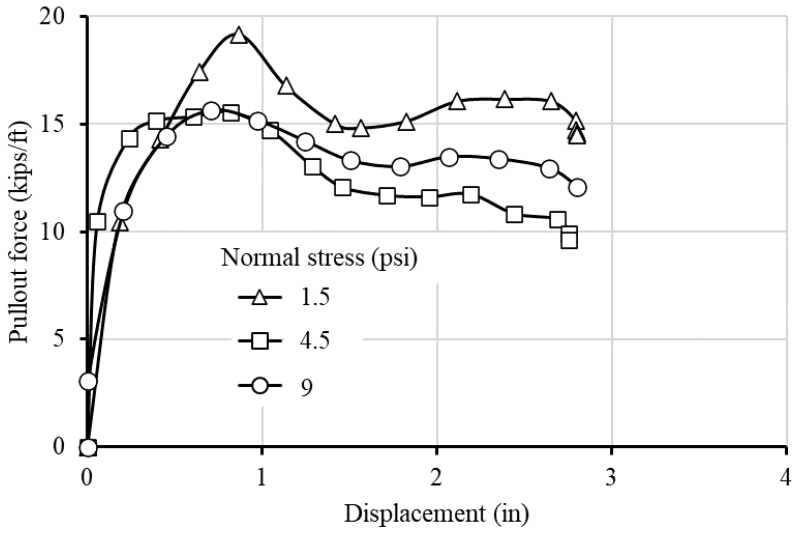

(b) Steel Strip-Reinforced LCC (100:0)

Figure 4.11: Pullout Force Versus Displacement for Steel Strip at the Age of 28 Days

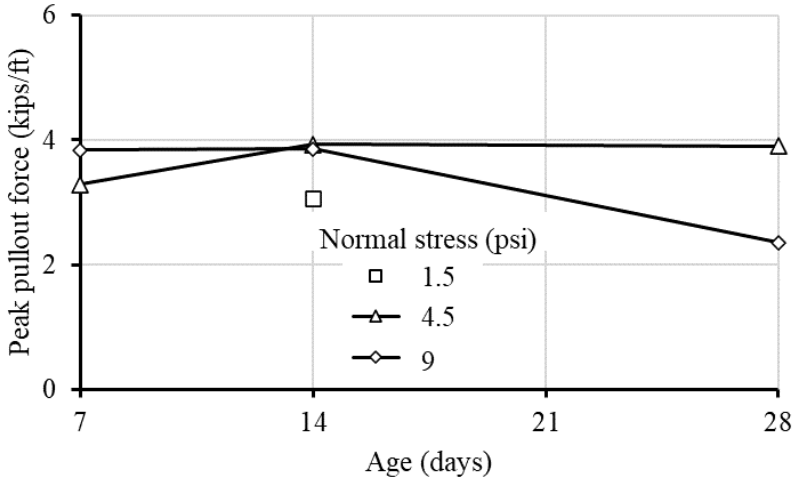

(a) Geogrid-Reinforced LCC (75:25)

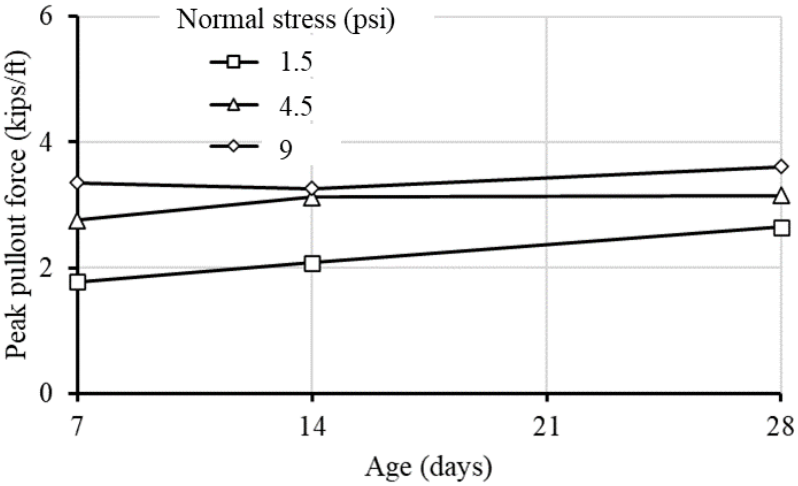

(b) Geogrid-Reinforced LCC (100:0)

Figure 4.12: Peak Pullout Force Versus Age for Geogrid in LCC

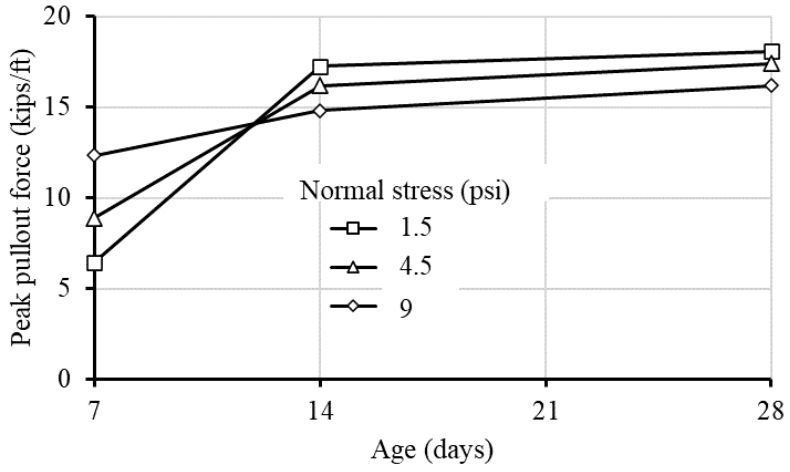

(a) Steel Strip-Reinforced LCC (75:25)

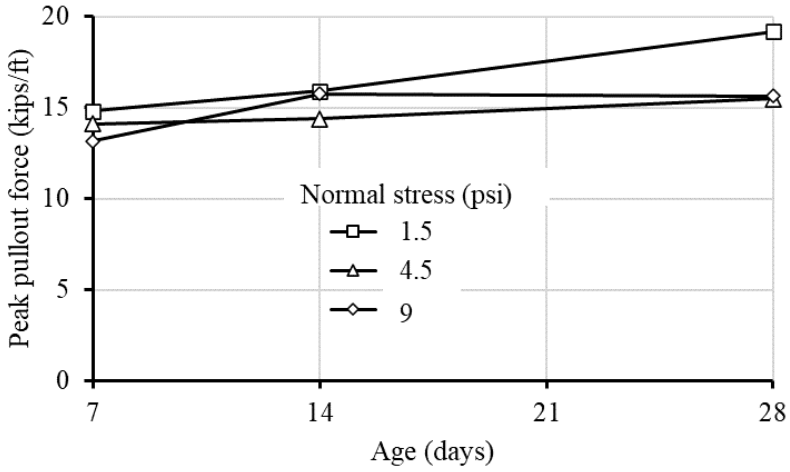

(b) Steel Strip-Reinforced LCC (100:0)

Figure 4.13: Peak Pullout Force Versus Age for Steel Strip in LCC

Figure 4.14 shows the front displacement versus rear displacement curves for pullout tests T26 and T32 as examples, but are representative of the behavior of all specimens in this study. Geogrid reinforcement was used in T26, while steel strip reinforcement was used in T32. For the geogrid reinforcement, the rear displacement increased negligibly relative to the front displacement up to a transition point corresponding to the slip extending to the rear of the reinforcement and then had a significant increase relative to the front displacement. In other words,

the whole length of the geogrid slipped under the pullout force after the transition point. At the transition point, the corresponding pullout force was close to the peak value. In this case, the bearing resistance of the transverse bar and the friction resistance of the longitudinal bar almost entered the critical state (i.e., the bearing and friction resistance fully developed). For the steel strip reinforcement, its front displacement was similar to the rear displacement throughout the test, owing to the relatively inelastic nature of the steel strip as compared to the geogrid.

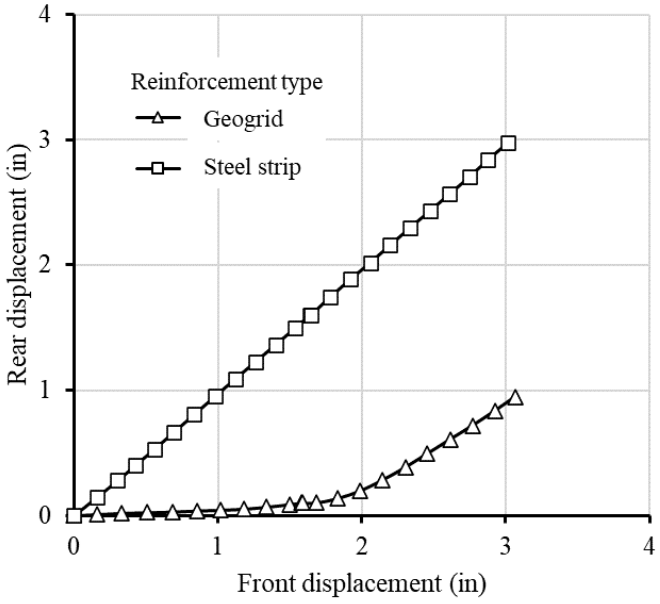

Figure 4.14: Front Displacement Versus Rear Displacement for Reinforcement

4.2.2 Effects of Cold Joint and Re-Pullout

Figure 4.15 shows the pullout force versus displacement for the reinforcement in the LCC (75:25) specimens with and without a cold joint under the normal stress of 4.5 psi at 7, 14, and 28 days. All specimens had steel strip reinforcement. The test results show that the pullout resistances for the reinforcement in the LCC specimens with a cold joint were higher than those without a cold joint, indicating that the cold joint did not reduce the pullout resistance of the steel strip embedded in LCC. In addition, the specimens with a cold joint required larger displacements to reach the peak pullout forces. This result may be attributed to the fact that the first lift of LCC hardened with

a rough surface before the placement of the second lift, resulting in an increased interface resistance.

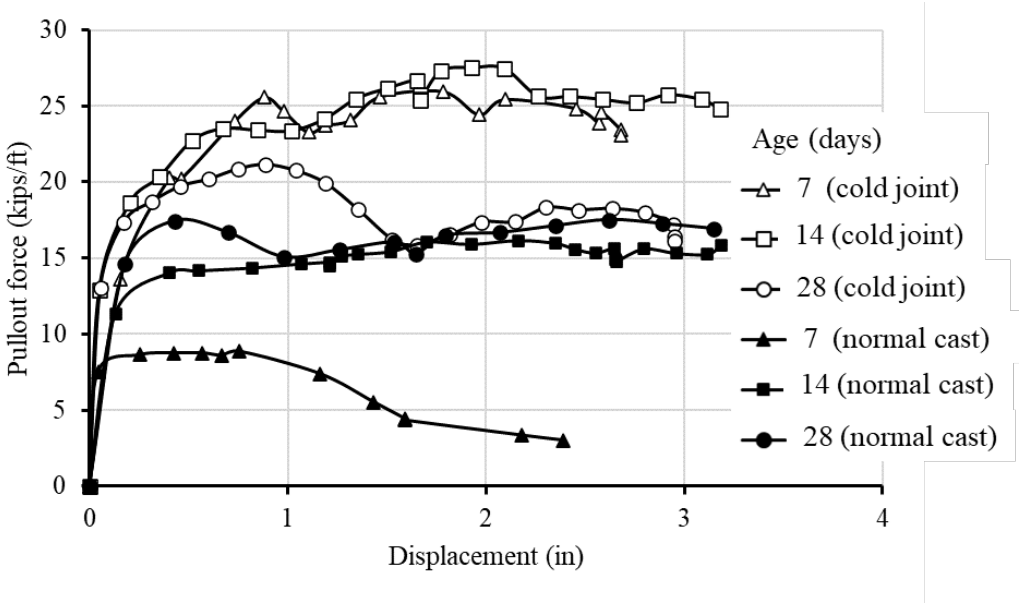

Figure 4.15: Pullout Force Versus Front Displacement for LCC (75:25) Specimens with Cold Joint and Normal Cast

To investigate the effect of earlier (original) pullout on later (repeat) pullout resistance, re-pullout tests were conducted on steel strip-reinforced and geogrid-reinforced LCC specimens. Figure 4.16a shows the variations of the re-pullout force versus the front displacement for the geogrid-reinforced LCC (75:25) specimens. These specimens were originally tested at 7 days and then re-tested at 35 days. Other comparable specimens tested at 28 days are also shown for the comparison purpose. It is shown that the peak re-pullout forces were 16% to 39% lower than those of the original tests on the same specimens at 7 days and 29.8% to 42% lower than those of the original tests on the different specimens at 28 days.

Figure 4.16b shows the variations of the re-pullout force versus the front displacement for the steel strip-reinforced LCC (75:25) specimens that were originally tested at 14 days and then re-tested at 35 days. It should be noted that Figure 4.16b has a different vertical scale from Figure 4.16a. Test results from other comparable specimens tested at 28 days (with no re-pullout) are also shown for the comparison purpose. The re-pullout initial force-displacement curves up to the peak

values were similar to those in the original pullout curves. However, the average peak pullout force of three re-pullout tests at 35 days was 14 kips/ft, which is slightly lower than 16 kips/ft from the original tests at 14 days and 17 kips/ft from the original tests at 28 days. The required displacement for the re-pullout force to reach the peak value was approximately 0.3 inch, which is smaller than those of the original tests. After the peak values, the pullout forces decreased sharply with the displacement. This comparison shows that the original pullout reduced the pullout resistance by 8.7% and the displacement required to reach the peak value decreased by 61.1%.

More significantly, the pullout force after the peak value dropped substantially. The difference in the behavior between the steel strip and geogrid in the re-pullout tests is likely because the geogrid sheared through almost the entire cross-section of the specimen during the original pullout test.

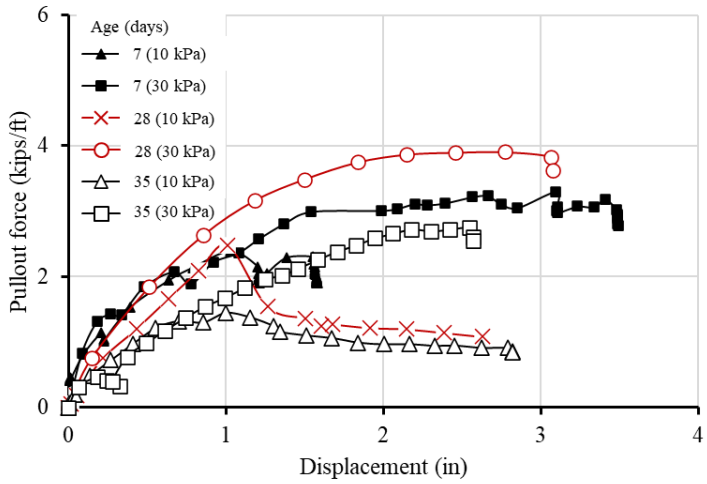

(a) Geogrid-Reinforced LCC (75:25)

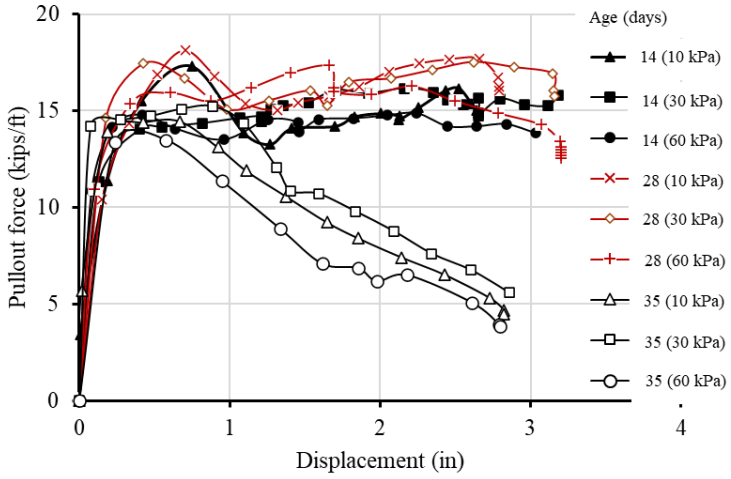

(b) Steel Strip-Reinforced LCC (75:25)

Figure 4.16: Pullout Force Versus Front Displacement for Repeat and Original Pullout Tests

4.2.3 Pullout Resistance Factor

As discussed in the introduction, Berg et al. (2009) suggested a pullout resistance factor F^* to calculate pullout resistance in design. Based on the pullout test results, the pullout resistance factor F^* for the geogrid and the steel strip embedded in LCC can be calculated using Equation

2.3. In the calculation, the scale effect correction factor α for geogrid was selected as 0.8, which is the average of the maximum value and the minimum value recommended by Berg et al. (2009). The scale effect correction factor α for the steel strip was 1.0.

Berg et al. (2009) also provided the formula to calculate the F^* factor for geosynthetic (i.e., geogrid and geotextile) reinforcement based on the peak friction angle of backfill as follows:

$$F^* = \frac{2}{3}\tan\varphi$$

Equation 4.1

Where: φ is the peak friction angle of MSE wall backfill.

Triaxial tests on LCC from Tiwari et al. (2017) found an effective friction angle of 34°. This angle is also suggested for a granular backfill by FHWA (Berg et al., 2009) if no test data is available. Therefore, it was adopted in this paper to calculate the F^* factor for the geogrid reinforcement as the reference line based on the FHWA recommendation for a granular backfill.

Figure 4.17 shows the variations of the pullout resistance factor F^* versus the normal stress for the geogrid-reinforced LCC tests conducted at 7, 14, and 28 days. Figure 4.17 compares the F^* factors for the geogrid embedded in LCC with the reference line from FHWA (Berg et al., 2009) based on Equation 4.1. Figure 4.17 shows that the F^* factor for the geogrid in the LCC backfill was greater than the reference line when the normal stress was lower than 4.5 psi but was similar to the reference line when at a normal stress of 9 psi. In addition, the F^* factor for the geogrid reinforced LCC decreased with normal stress.

Figure 4.18 shows the variations of the pullout resistance factor F^* versus the normal stress for the steel strip-reinforced LCC tests conducted at the ages of 7, 14, and 28 days. FHWA (Berg et al., 2009) also provided a relationship to calculate the F^* factor for the steel ribbed reinforcement based on the internal friction angle and the uniformity coefficient of backfill as follows:

At the top of the wall:

$$F^* = 1.2 + \log C_u \leq 2$$

Equation 4.2

At a depth of 20 feet and below:

$$F^* = \tan \varphi$$

Equation 4.3

Where: C_u is the uniformity coefficient of the backfill and φ is the angle of internal friction of the backfill.

For the design of an MSE wall, when C_u and φ for the specific backfill are unknown, AASHTO (2012) suggested that C_u and φ should be selected as 4 and 34°. Considering the typical density of backfill for MSE walls is 127 pcf, the calculated normal stress at the depth of 20 feet is 17 psi. AASHTO (2012) suggested that the calculated F^* factor for steel ribbed reinforcement using the relationship from FHWA (Berg et al., 2009) decreases linearly from the top of the wall (at a normal stress of 0 psi) to a depth of 20 feet (at a normal stress of 17 psi).

Figure 4.18c compares the F^* factors for the steel strip embedded in LCC, aggregate (Weldu, Han, Rahmaninezhad, Parsons, & Kakrasul, 2015), sand (Rahmaninezhad et al., 2019), and the reference line from FHWA (Berg et al., 2009) based on Equations 4.2 and 4.3. Figure 4.18 shows that for the steel strip-reinforced LCC, the F^* factor decreased as the normal stress increased. This trend is consistent with those for the aggregate, the sand, and the reference line. Other researchers (Jayawickrama, Surles, Wood, & Lawson, 2013; Jayawickrama, Lawson, Wood, & Surles, 2015) observed similar behavior for aggregate backfills. The reason for the larger F^* factor at a low normal stress is that dilation of backfill is more likely to occur at that depth (Weldu et al., 2015). However, F* slightly increased with age due to the increase of the strength of LCC. Figure 4.18c also shows that the F^* factors for LCC were larger than those for the aggregate, the sand, and the reference line when the normal stress was lower than 3.5 psi. When the normal stress ranged from 3.5 to 9 psi, the F^* factor for LCC was similar to those for aggregates. Figure 4.18c also shows the F^* for the aggregate was larger than that of the sand. In addition, the F^* factor for the steel strip reinforced LCC was larger than that for the geogrid-reinforced LCC, which is similar to that suggested by FHWA (Berg et al., 2009).

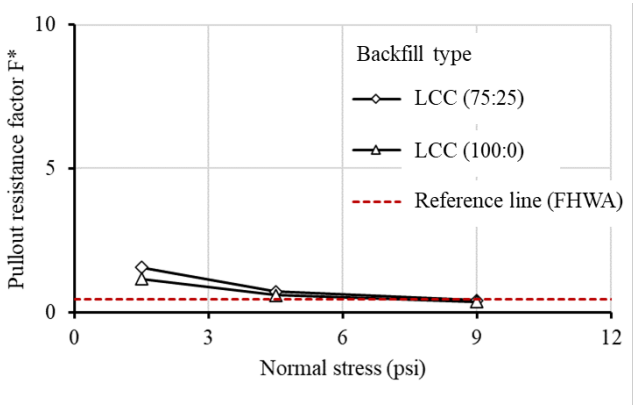

(a) 7 Days

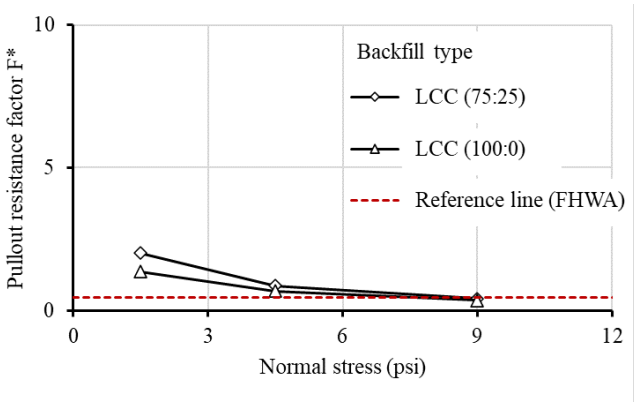

(b) 14 Days

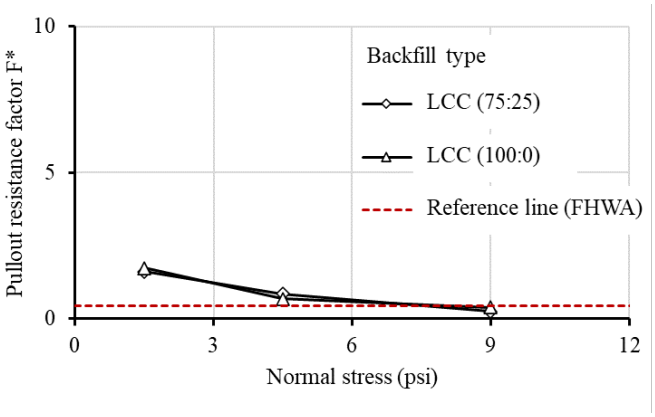

(c) 28 Days

Figure 4.17: Pullout Resistance Factor F* Versus Normal Stress for Geogrid-Reinforcement at: (a) 7 Days, (b) 14 Days, and (c) 28 Days

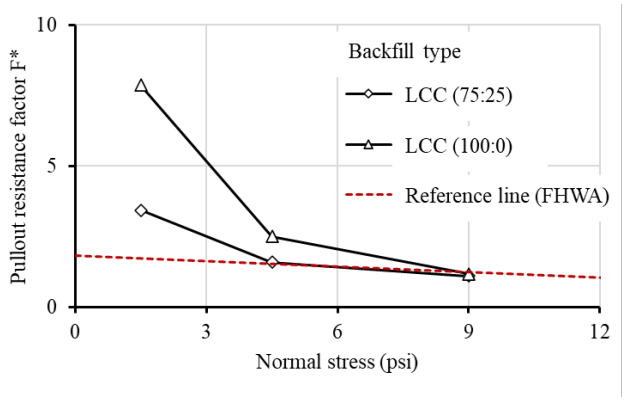

(a) 7 Days

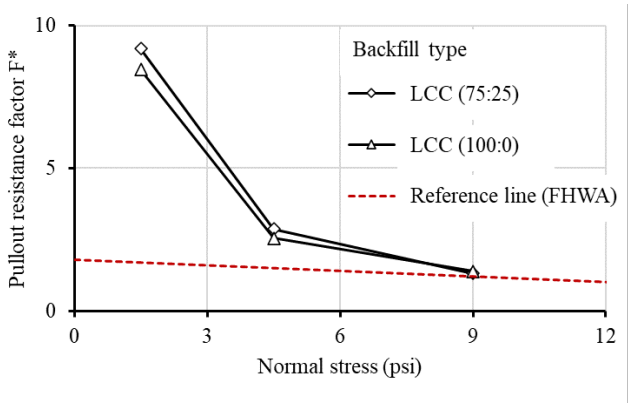

(b) 14 Days

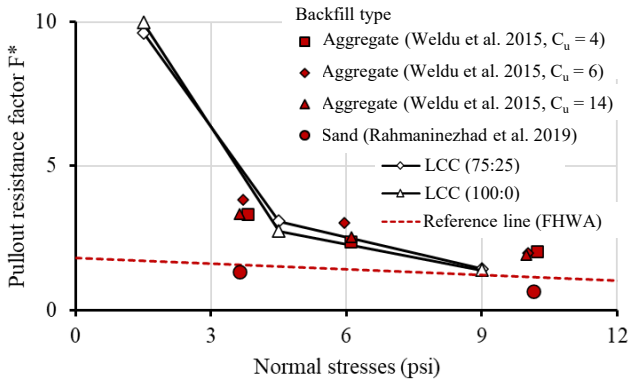

(c) 28 Days

Figure 4.18: Pullout Resistance Factor F* Versus Normal Stress for Steel Strip-Reinforcement at: (a) 7 Days, (b) 14 Days, and (c) 28 Days

Chapter 5: Conclusions and Recommendations

5.1 Conclusions

This report presents a series of laboratory tests to evaluate the material properties of LCC and the pullout resistances of geogrid and steel strip in LCC specimens cast in the field. Based on the test results, the following conclusions can be drawn:

1. The average wet densities of LCC ranged from 30 to 36 pcf at the age of 28 days and the average dry densities ranged from 21 to 24 pcf at the same age. The dry density was approximately 67% of the wet density. The density increased as the cement to fly ash ratio increased. All LCC specimens used in this study are considered ultra-low density cellular concrete.
2. The permeability values for LCC measured using the falling head method ranged from 2.1×10^{-5} to 3.0×10^{-4} in./s, respectively. In general, the permeability decreased as the hydraulic gradient and the confining stress increased.
3. For the small shear box tests, the cohesion values of the LCC specimens ranged from 19 to 37 psi, while their frictional angles ranged from 19 to 63 degrees. For the large shear box tests, the cohesion values of the LCC specimens ranged from 33 to 50 psi, while their frictional angles ranged from 23 to 79 degrees. The large shear box tests measured higher shear strengths than the small shear box tests.
4. The measured elastic moduli and Poisson's ratios of the LCC specimens ranged from 189 to 286 ksi and 0.34 to 0.35, respectively. The measured average compressive strengths ranged from 62 to 167 psi at the age of 28 days. The compressive strength increased as the age and the cement to fly ash ratio increased. The measured compression indices $C_{c\varepsilon}$ and recompression indices $C_{r\varepsilon}$ ranged from 4.1×10^{-2} to 1.1×10^{-1} and 6.2×10^{-3} to 7.2×10^{-3}, respectively.

5. The pullout response of the geogrid in LCC at high normal stress showed hardening behavior, while the geogrid-reinforced LCC at low normal stress showed softening behavior. The pullout response of the steel reinforcement in LCC showed softening behavior in all cases.
6. The pullout resistances of geogrid and steel reinforcement in the LCC specimens increased as the cement to fly ash ratio increased. The normal stress had an obvious effect on the pullout resistance of geogrid in LCC but a limited effect on the pullout resistance of steel strip in LCC. The LCC specimens with a higher cement to fly ash ratio had a more rapid strength gain, resulting in an increase in the pullout resistance within a shorter time.
7. In this study, the presence of a cold joint did not reduce the pullout resistance of the steel strip-reinforced LCC. Re-pullout slightly reduced the pullout resistance of the steel strip-reinforced LCC, but more dramatically reduced the pullout resistance of the geogrid-reinforced LCC. Steel reinforcement exhibited significant softening behavior under re-pullout, whereas geogrid reinforcement did not.
8. The pullout resistance factors F^* for geogrid and steel-reinforced LCC decreased as the normal stress increased, but increased with age. In addition, the F^* factor for the geogrid embedded in LCC was larger than the FHWA reference line with a typical backfill friction angle of 34°, while the F^* factor for the steel strip embedded in LCC was larger than that in the aggregate, the sand, and the FHWA reference line when the normal stress was lower than 3.5 psi.

5.2 Recommendations for Future Projects and Studies

Based on the above conclusions, the following recommendations can be made for future projects:

1. LCC can be used as a backfill material alternative to granular backfill materials for MSE wall construction with steel strips and geogrid reinforcements.
2. It is conservative to use the current FHWA design method for estimating the pullout resistances of steel strips and geogrid reinforcements in LCC using a backfill friction angle of 34^{o}.
3. LCC is less permeable than typical granular backfill materials used for MSE walls; therefore, drainage is needed behind the LCC block.

To better understand the performance of LCC as a backfill material for MSE walls beyond what were investigated in this study, the following recommendations are made for future studies:

1. This study focused on LCC for MSE walls under regular conditions; however, LCC may be subjected to freeze-thaw cycles. It is recommended that the effects of freeze-thaw cycles on the material properties of LCC should be investigated.
2. The elastic modulus, internal friction angle, and cohesion predicted using the correlations in the literature did not match the measured values for the LCC specimens, especially with the addition of fly ash. It is recommended that new correlations for these material properties of LCC with fly ash should be developed.
3. LCC may be used in MSE walls to support footings. There is limited information on the bearing capacity of LCC as a foundation material. To facilitate the application of LCC in MSE walls as a foundation material, the bearing capacity of unreinforced and reinforced LCC foundations should be investigated.

References

AASHTO. (1993). *Guide for design of pavement structures*. Washington, DC: American Association of State Highway and Transportation Officials.

AASHTO. (2012). *AASHTO LRFD bridge design specifications* (6th ed.). Washington, DC: American Association of State Highway and Transportation Officials.

American Concrete Institute (ACI) Committee 523. (2006). *Guide for cast-in-place low density cellular concrete*. Farmington Hills, MI: American Concrete Institute.

Aldridge, D. (2005). Introduction to foamed concrete: what, why, how? Use of foamed concrete in construction. In *Proceedings of the International Conference held at the University of Dundee* (pp. 1-14). Thomas Telford Publishing, Scotland, UK.

Alfaro, M. C., Hayashi, S., Miura, N., & Watanabe, K. (1995). Pullout interaction mechanism of geogrid strip reinforcement. *Geosynthetics International, 2*(4), 679–698.

ASTM C39/C39M. (2021). *Standard test method for compressive strength of cylindrical concrete specimens*. West Conshohocken, PA: ASTM International.

ASTM C39/C39M-16b. (2015). *Standard test method for compressive strength of cylindrical concrete specimens*. West Conshohocken, PA: ASTM International.

ASTM C511-21. (2021). *Standard specification for mixing rooms, moist cabinets, moist rooms, and water storage tanks used in the testing of hydraulic cements and concretes*. West Conshohocken, PA: ASTM International.

ASTM D2435/D2435M-11. (2011). *Standard test methods for one-dimensional consolidation properties of soils using incremental loading*. West Conshohocken, PA: ASTM International.

ASTM D3080-11. (2011). *Standard test method for direct shear tests of soils under consolidated drained conditions*. West Conshohocken, PA: ASTM International.

ASTM D5084-10. (2010). *Standard test methods for measurement of hydraulic conductivity of saturated porous materials using a flexible wall permeameter*. West Conshohocken, PA: ASTM International.

ASTM D6706-01. (2013). *Standard test method for measuring geosynthetic pullout resistance in soil*. West Conshohocken, PA: ASTM International.

Baena, M., Torres, L., Turon, A., & Barris, C. (2009). Experimental study of bond behavior between concrete and FRP bars using a pull-out test. *Composites Part B: Engineering, 40*(8), 784–797.

Ben-Romdhane, M. R., & Ulm, F. J. (2002). Computational mechanics of the steel–concrete interface. *International Journal for Numerical and Analytical Methods in Geomechanics, 26*(2), 99–120.

Berg, R. R., Samtani, N. C., & Christopher, B. R. (2009). *Design of mechanically stabilized earth walls and reinforced soil slopes–volume II* (Report No. FHWA-NHI-10-025). Washington, DC: Federal Highway Administration.

Bergado, D. T., & Chai, J. (1994). Pullout force/displacement relationship of extensible grid reinforcements. *Geotextiles and Geomembranes, 13*(5), 295–316.

Bouazaoui, L., & Li, A. (2008). Analysis of steel/concrete interfacial shear stress by means of pullout test. *International Journal of Adhesion and Adhesives, 28*(3), 101–108.

Canadian Geotechnical Society. (2006). *Canadian foundation engineering manual (CFEM)*. BiTech Publisher Ltd, Richmond, BC, Canada: Canadian Geotechnical Society.

Engineered Fill. (2001). *Elastizell EF (engineered fill) geotechnical applications*. Elastizell Corp., p. 16.

Esfandiari, J., & Selamat, M. R. (2012). Laboratory investigation on the effect of transverse member on pull out capacity of metal strip reinforcement in sand. *Geotextiles and Geomembranes, 35*, 41–49.

Han, J. (2015). *Principles and Practice of Ground Improvement*. John Wiley & Sons Publishing.

Hulimka, J., Krzywoń, R., & Knoppik-Wróbel, A. (2011). Use of foamed concrete in the structure of passive house foundation slab. In *Proceedings of the 7th International Conference on Analytical Models and New Concepts in Concrete and Masonry Structures AMCM2011* (pp. 221–222). Wydawnictwo Politechniki Krakowskiej.

Jalal, M. D., Tanveer, A., Jagdeesh, K., & Ahmed, F. (2017). Foam concrete. *International Journal of Civil Engineering Research, 8*(1), 1–14.

Jayawickrama, P. W., Lawson, W. D., Wood, T. A., & Surles, J. G. (2015). Pullout resistance factors for steel MSE reinforcements embedded in gravelly backfill. *Journal of Geotechnical and Geoenvironmental Engineering, 141*(2), 04014090.

Jayawickrama, P. W., Surles, J. G., Wood, T. A., & Lawson, W. D. (2013). *Pullout resistance of MSE reinforcement in backfills typically used in Texas* (Report No. FHWA/TX-13/0-6493-R1, Vol. 1). Austin, TX: Texas Department of Transportation.

Jones, M. R. (2001). Foamed concrete for structural use. In *Proceedings of one day seminar on foamed concrete: Properties, applications and latest technological developments* (pp. 27–60). Loughborough University.

Jones, M. R., & McCarthy, A. (2005a). Behaviour and assessment of foamed concrete for construction applications. Use of foamed concrete in construction. In *Proceedings of the International Conference held at the University of Dundee* (pp. 61–88). Thomas Telford Publishing, Scotland, UK.

Jones, M. R., & McCarthy, A. (2005b). Preliminary views on the potential of foamed concrete as a structural material. *Magazine of Concrete Research, 57*(1), 21–31.

Jones, M. R., & McCarthy, A. (2006). Heat of hydration in foamed concrete: Effect of mix constituents and plastic density. *Cement and Concrete Research, 36*(6), 1032–1041.

Juenger, M. C. G., Winnefeld, F., Provis, J. L., & Ideker, J. H. (2011). Advances in alternative cementitious binders. *Cement and Concrete Research, 41*(12), 1232–1243.

Kearsley, E. P., & Mostert, H. F. (2005). Designing mix composition of foamed concrete with high fly ash contents. In *Use of foamed concrete in construction*: *Proceedings of the International Conference held at the University of Dundee* (pp. 29-36). Thomas Telford Publishing, Scotland, UK.

Kearsley, E. P., & Wainwright, P. J. (2001). The effect of high fly ash content on the compressive strength of foamed concrete. *Cement and Concrete Research, 31*(1), 105–112.

Kim, H. K., Jeon, J. H., & Lee, H. K. (2012). Workability, and mechanical, acoustic and thermal properties of lightweight aggregate concrete with a high volume of entrained air. *Construction and Building Materials, 29*, 193–200.

Lee, M. Y., Hardy, R. D., & Bronowski, D. R. (2004). *Laboratory constitutive characterization of cellular concrete*. Oak Ridge, TN: Department of Energy.

Lim, S. K., Tan, C. S., Lim, O. Y., & Lee, Y. L. (2013). Fresh and hardened properties of lightweight foamed concrete with palm oil fuel ash as filler. *Construction and Building Materials, 46*, 39–47.

Liu, X., Ni, C., Meng, K., Zhang, L., Liu, D., & Sun, L. (2020). Strengthening mechanism of lightweight cellular concrete filled with fly ash. *Construction and Building Materials, 251*, 118954.

Liu, S., Zhu, D., Wang, X., & Shi, C. (2019). Pullout properties of AR-glass textile embedded in cement matrix under different velocities and temperatures. *Construction and Building Materials, 228*, 116779.

Ma, C., & Chen, B. (2015). Properties of a foamed concrete with soil as filler. *Construction and Building Materials, 76*, 61–69.

McCormick, F. C. (1967). Rational proportioning of preformed foam cellular concrete. *ACI Material Journal, 64*(2), 104–110.

Mindess, S. (2019). *Developments in the formulation and reinforcement of concrete*. Woodhead Publishing.

Mohd, S. K. A., & Mohammed, S. A. R. (2017). Applications of foamed lightweight concrete. *MATEC Web of Conferences, 97*(01097), 1–5.

Moraci, N., Cardile, G., Gioffrè, D., Mandaglio, M. C., Calvarano, L. S., & Carbone, L. (2014). Soil geosynthetic interaction: Design parameters from experimental and theoretical analysis. *Transportation Infrastructure Geotechnology, 1*(2), 165–227.

Morsy, A. M., Zornberg, J. G., Han, J., & Leshchinsky, D. (2019). A new generation of soil-geosynthetic interaction experimentation. *Geotextiles and Geomembranes, 47*(4), 459–476.

Narayanan, N., & Ramamurthy, K. (2000). Structure and properties of aerated concrete: A review. *Cement and Concrete Composites, 22*(5), 321–329.

Naval Facilities Engineering Command. (1982). *Soil Mechanics: Design Manual 7.1*. Naval Facilities Engineering Command. Alexandria, VA: Department of the Navy.

Ni, F. M. W., Oyeyi, A. G., & Tighe, S. (2020). The potential use of lightweight cellular concrete in pavement application: A review. *International Journal of Pavement Research and Technology, 13*(6), 686–696.

Ozlutas, K. (2015). *Behaviour of ultra-low density foamed concrete* (Doctoral dissertation). Division of Civil Engineering, University of Dundee.

Palmeira, E. M., & Milligan, G. W. E. (1989). Scale and other factors affecting the results of pull-out tests of grid buried in sand. *Geotechnique 39*(3), 511–524.

Panesar, D. K. (2013). Cellular concrete properties and the effect of synthetic and protein foaming agents. *Construction and Building Materials, 44*, 575–584.

Rahmaninezhad, S. M., Han, J., Kakrasul, J. I., & Weldu, M. (2019). Stress distributions and pullout responses of extensible and inextensible reinforcement in soil using different normal loading methods. *Geotechnical Testing Journal, 42*(6), 1606–1623.

Ramamurthy, K., Nambiar, E. K., & Ranjani, G. I. S. (2009). A classification of studies on properties of foam concrete. *Cement and Concrete Composites, 31*(6), 388–396.

Ramezani, M., Vilches, J., & Neitzert, T. (2013). Pull-out behavior of galvanized steel strip in foam concrete. *International Journal of Advanced Structural Engineering, 5*(1), 24.

Rao, F., Zhang, Z., Ye, G., Liu, J., & Han, J. (2021). Mesostructure of foamed cement paste and its influence on macromechanical behavior. *Journal of Materials in Civil Engineering, 33*(6), 04021114.

Soil Exploration Company. (1981). *Permeability tests low density Elastizell concrete cylinders* (Project No. 120–7690). St Paul, MN.

Sukmak, K., Sukmak, P., Horpibulsuk, S., Han, J., Shen, S. L., & Arulrajah, A. (2015). Effect of fine content on the pullout resistance mechanism of bearing reinforcement embedded in cohesive-frictional soils. *Geotextiles and Geomembranes, 43*, 107–117.

Tada, S. (1986). Material design of aerated concrete—An optimum performance design. *Materials and Structures, 19*(1), 21–26.

Tian, W., Li, L., Zhao, X., Zhou, M., & Wang, N. (2009). Application of foamed concrete in road engineering. In *International Conference on Transportation Engineering* (pp. 2114–2120).

Tiwari, B., Ajmera, B., Maw, R., Cole, R., Villegas, D., & Palmerson, P. (2017). Mechanical properties of lightweight cellular concrete for geotechnical applications. *Journal of Materials in Civil Engineering, 29*(7), 06017007.

Tran, V. D. H., Meguid, M. A., & Chouinard, L. E. (2013). A finite–discrete element framework for the 3D modeling of geogrid–soil interaction under pullout loading conditions. *Geotextiles and Geomembranes, 37*, 1–9.

Transportation Association of Canada. (2013). *Transport asset design and management guide*. Ottawa, Ontario, Canada: Transportation Association of Canada.

Watabe, Y., & Noguchi, T. (2011). Site-investigation and geotechnical design of D-runway construction in Tokyo Haneda Airport. *Soils and Foundations, 51*(6), 1003–1018.

Weldu, M. T., Han, J., Rahmaninezhad, S. M., Parsons, R. L., & Kakrasul, J. I. (2015). *Pullout resistance of mechanically stabilized earth wall steel strip reinforcement in uniform aggregate* (Report No. K-TRAN: KU-14-7). Lawrence, KS: University of Kansas.

Yakovlev, G., Kerienė, J., Gailius, A., & Girnienė, I. (2006). Cement based foam concrete reinforced by carbon nanotubes. *Materials Science [Medžiagotyra], 12*(2), 147–151.

Yang, Y., & Chen, B. (2016). Potential use of soil in lightweight foamed concrete. *KSCE Journal of Civil Engineering, 20*(6), 2420–2427.

K-TRAN

KANSAS TRANSPORTATION RESEARCH AND NEW-DEVELOPMENT PROGRAM

AD ASTRA PER ASPERA

Kansas

Department of Transportation